

## 平成 年度共同利用実施報告書(研究実績報告書)

## 1. 共同利用種目(該当種目にチェック)

特定共同研究(A)      特定共同研究(B)      特定共同研究(C)      一般共同研究  
 地震・火山噴火予知研究      施設・実験装置・観測機器等の利用  
 データ・資料等の利用      研究会

2. 課題番号または共同利用コード      2009 - A - 14

## 3. プロジェクト名、研究課題、集会名、または利用施設・装置・機器・データ等の名称

和文：火山噴火素過程としてのマグマの分化・発泡・脱ガス過程の研究

英文：Studies on elementary processes of volcanic eruptions

4. 研究代表者所属・氏名 九州大学大学院理学研究院・寅丸敦志

(地震研究所担当教員名) (中田節也・市原美恵)

## 5. 利用者・参加者の詳細(研究代表者を含む。必要に応じ行を追加すること)

氏名	所属・職名	利用・参加内容または 施設,装置,機器,データ	利用・参加期間	日 数	旅費 支給
寅丸敦志	九州大学・教授	研究会主催・発表	2010/02/07-09	3	無し
中村美千彦	東北大学・准教授	研究会参加・発表	2010/02/08	1	無し
西村太志	東北大学・准教授	研究会参加・発表	2010/02/08	1	無し
吉田茂生	名古屋大学・准教授	研究会参加	2010/02/08	1	無し
市原美恵	東京大学・助教	研究会参加・発表	2010/02/08	1	無し

## 6. 研究内容(コンマ区切りで3つ以上のキーワードおよび400字程度の成果概要を記入)

キーワード：素過程、発泡、脱ガス、マグマ破壊

次期噴火予知計画では、地震予知計画と連携すると共に、これまでの予知計画にはなかった噴火素過程という項目が新たに付け加えられた。近年、活動的火山の観測・監視が多項目化し、多様な観測情報が得られるようになったものの、それらの情報を有機的に結びつけるための物理モデル構築とそれらを支配する「素過程」の理解が必要とされてきた。本研究の目的は、個々の素過程の噴火現象における役割を確認することにより、噴火現象の総合的理解へと結びつけることにある。今年度は、平成22年2月8日に、地震研究所において、研究会を開催し、以下のテーマについて研究発表、及び、討論を行った。「マグマ破壊の脆性度を定めるパラメータ」(地震研・市原美恵)。「物質科学的な噴火様式・推移予測の展望」(東北大学・中村美千彦ほか)。「浅部火山性流体挙動の理論的研究」(東北大学・西村太志)。「間欠泉実験から見た長期予測と短期予測」(九州大学・前田一樹、寅丸敦志)。なお、共同利用研究費として、12万円が配分されていたが、この研究会に旅費支給の要望がなかったため、使用をしなかった。

7 . 研究実績報告（公表された成果のリスト<sup>\*1</sup>または2000～3000字の報告書）

（<sup>\*1</sup>論文タイトル、雑誌・学会・セミナー等の名称、謝辞への記載の有無、ポイント数、電子ファイル添付のこと）

Nishimura, T., Volcano deformation caused by magma ascent in an open conduit, *J. Volcanol. Geotherm. Res.*, 187, 178-192, 2009. 謝辞に記載無し、3点

市原美恵, 佐藤元彦, 宮林佐和子, 武尾実, 綿田辰吾, 井口正人, 木管楽器(リコーダー)に学ぶ火山性微動発生機構の考察, 日本火山学会秋季大会(2009-10.10, 神奈川県立生命の星・地球博物館), B11, 謝辞に記載無し、2点

## 報告書（様式6）作成にあたってのお願い

- ・必ず電子ファイルで提出してください。
- ・「5.利用者・参加者の詳細」については、当該共同利用の利用者・（研究集会を含む）参加者全員について個別に、氏名・所属・職名・利用内容・期間（利用のあった年月日）・合計日数・旅費支給の有無を記入してください。必要に応じて表の行を追加してください。
- ・「7.研究実績報告」には、原則として公表された成果（投稿済も可）のリストを書いてください。雑誌への投稿、学会講演等を以下の要領でポイント化し、研究種目ごとに決められたポイントを満たす「成果のリスト」をもって研究実績報告とします。ポイントを満たさない場合、2,000字～3,000字の報告書をもって「研究実績報告」としてください。
- ・「成果のリスト」に記載した論文、学会講演予稿などは電子ファイルも提出してください（未受理のものを除く）。提出された資料は共同利用の内部資料として保存し公開はしません。

## ポイント表

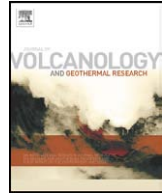
	謝辞に記載あり	謝辞に記載なし
雑誌への投稿	6	3
学会講演	4	2
地震研究所内発表（談話会・金曜日セミナー等）	1	-
（研究集会）プロシーディングスの公開	5	3
（研究集会）予稿集の公開	5	3

## 「成果の公表」をもって研究実績報告とするための必要ポイント数

特定共同研究(A)	4
特定共同研究(B)	10
特定共同研究(C)	2
一般共同研究	5
施設・実験装置・観測機器等の利用	3
データ・資料等の利用	3
研究集会	5

## 研究成果公表にあたってのお願い

- ・研究成果を論文等で発表される場合、以下の形式の文章を謝辞等に記載して下さい。  
(英文)This study was supported by the Earthquake Research Institute cooperative research program.  
(和文)本研究は、東京大学地震研究所共同研究プログラムの援助をうけました。
- ・研究集会の場合は、以下の形式の文章を予稿集またはプロシーディングスに記載して下さい。  
(英文)This meeting was supported by the Earthquake Research Institute cooperative research program.  
(和文)本研究集会は、東京大学地震研究所共同研究プログラムの援助をうけました。
- ・研究成果について、本所の談話会、セミナー、「広報」での発表を歓迎いたします。



# Ground deformation caused by magma ascent in an open conduit

Takeshi Nishimura\*

Department of Geophysics, Graduate School of Science, Tohoku University, Aramaki-aza Aoba 6-3, Aoba-ku, Sendai 980-8578, Japan

## ARTICLE INFO

### Article history:

Received 1 August 2008

Accepted 1 September 2009

Available online 12 September 2009

### Keywords:

ground deformation  
eruption  
open conduit  
magma  
gas bubble

## ABSTRACT

This study examines magma ascent processes of three basic types prior to intermittent explosions such as Vulcanian or Strombolian types: specifically their relations to volcano ground deformation. Such repetitive explosions eject magma from an open conduit at short time intervals. Consequently, magma pressure is expected to decrease at the conduit and/or reservoir, and thereby deflate the volcano. Then, magma within the conduit rises, exerting normal and shear stresses on the conduit wall, thereby inflating the volcano. Diffusive mass transfer of water molecules from the melt to bubbles might occur subject to a sudden depressurization by eruption when magma includes numerous small gas bubbles. Such gas bubble expansion lifts the magma in the conduit. Calculations of ground deformation on a semi-infinite medium for such rising magma show that vertical and radial displacements and tilt motions recorded in the far fields are proportional to the 1.5 power of time. For low-viscosity magma, gas bubbles might rise in the melt because of buoyancy force. The gas bubbles expand rapidly with time because of decreased ambient pressure, pushing the magma upward in the conduit. Consequently, the volcano slowly inflates initially; then the rate of deformation increases over time, eventually engendering a rapid inflation immediately before eruption. These temporal changes in ground deformations contrast against cases in which magma does not include gas bubbles. In such cases, amplitudes of ground deformation increase almost linearly or even decrease with time at far fields. These differences, which are recognized as basic characteristics of temporal changes of ground deformation, enable us to know the driving forces of magma in an open conduit and to evaluate the gas bubble behavior quantitatively in magma before eruption.

© 2009 Elsevier B.V. All rights reserved.

## 1. Introduction

Behaviors of volatiles included in magma are well known to play important roles in volcanic activity, eruption styles, and intensities. For that reason, many theoretical models, numerical calculations, laboratory experiments, and geologic sample analyses have been conducted intensively to elucidate volatile behavior. For example, nucleation and bubble growth processes of volatiles in magma are represented by equations incorporating physical parameters such as the melt viscosity, diffusion coefficient of H<sub>2</sub>O/CO<sub>2</sub> molecules in the melt, Henry's constant, surface tension, and confining pressure. These processes are triggered and accelerated by magma depressurization and crystallization (e.g., Toramaru, 1989; Prousevitch et al., 1993; Tait et al., 1989; Lensky et al., 2004; Shimomura et al., 2006). Laboratory experiments using geologic samples have elucidated the basic processes of nucleation, gas bubble growth and deformation, and degassing (e.g., Lyakhovskiy et al., 1996; Takeuchi et al., 2005; Okumura et al., 2006). Theoretical modeling of the conduit flow has been conducted to characterize macro-scale phenomena of volcanic explosions and eruptions (e.g., Jaupart and Allègre, 1991; Woods and

Koyaguchi, 1994; Prousevitch and Sahagian, 1996; Yoshida and Koyaguchi, 1999; Mason et al., 2006; Ida, 2007).

Volatile behaviors in magma are also discussed using geophysical data observed at active volcanoes. The cyclic behavior recorded in tilt records obtained at Soufriere Hills, Montserrat volcano (Voight et al., 1999), has been examined for nonlinear behavior of conduit flow attributable to crystallization and gas loss by permeable flow (Melnik and Sparks, 1999) and viscosity dependence on the volatile contents of the magma (Wylie et al., 1999). Such periodic behavior that is displayed by continuous discharges of lava dome eruptions has been examined also from nonlinear dynamics of conduit flows (Barmin et al., 2002; Nakanishi and Koyaguchi, 2008). Models including interaction of gas bubble growth processes with the surrounding elastic rocks (Nishimura, 2004; Chouet et al., 2006; Shimomura et al., 2006) enable us to relate microscale phenomena quantitatively with seismic and geodetic data. Results of those studies suggest pressure recovery processes in magma subject to sudden depressurization. Voight et al. (2006), based on analyses of borehole strain meter data, reported that such pressure recovery might have occurred at Soufriere Hills, Montserrat when a large amount of lava dome collapsed from the summit and reduced the static pressure of the magma chamber in a deep region. Ground deformation immediately preceding volcanic explosions has also been examined in terms of the gas bubble expansion process. Nishimura (2006) presented a simple ascent

\* Tel.: +81 22 795 6532; fax: +81 22 795 6783.  
E-mail address: [nishi@zisin.geophysics.tohoku.ac.jp](mailto:nishi@zisin.geophysics.tohoku.ac.jp).

model of magma in which gas bubble growth and out-gassing processes are considered, demonstrating that accelerated ground inflation precedes volcanic explosions, whereas gradual inflation is observed during non-explosive eruptions. These characteristics in temporal changes of ground deformation are recognized at four-fifths of active volcanoes, such as Mount St. Helens, Merapi, Montserrat, and Unzen (Dzurizin et al., 1983; Saito et al., 1993; Jackson et al., 1998; Yamashina and Shimizu, 1999; Voight et al., 2000). The results reported in those earlier studies strongly suggest that monitoring of volatile behaviors by geophysical techniques is quite useful not only to elucidate gas bubble growth mechanisms in magma but also to predict volcanic explosivity. Moreover, these studies shed new light on geodetic data that have been used mainly to determine the locations and sizes of intruded dikes or volcanic pressure sources by application of a spherical pressure source model (Mogi, 1958) or tensile dislocation model (Okada, 1992).

Recently, volcano inflations preceding small explosions that occur repeatedly have been reported at active volcanoes. Iguchi et al. (2008), by deploying broadband seismometers set at near an active vent, detected a small inflation of about  $50\mu\text{m}$  that occurs, by a few to 10 min, before small Vulcanian explosions at Suwanose-jima in Japan. Similar miniscule inflations preceding explosions are also detected: at Sumeru volcano in Indonesia, the repetitive tilt changes by about  $0.1\mu\text{rad}$ , where small Vulcanian explosions occur repeatedly every 5–10 min (Nishi et al., 2007; Iguchi et al., 2008). At Stromboli volcano in Italy, Ripepe and Harris (2008) reported a strong tilt component in broadband seismic signals that show conduit expansions at least 90 s before the explosion of April 5, 2003. Tiltmeters embedded at about 6 m depth detect tiny changes of upward tilting toward the vent with an order of  $10\text{nrad}$  before small explosions (Ripepe et al., personal communications). These ground deformations preceding small Vulcanian and Strombolian explosions at active volcanoes often seem to show slightly accelerated changes over time. On the other hand, such characteristics are not included in tilt records observed at Onikobe geyser (Nishimura et al., 2006). Because the mechanism of water effusion at geysers (depressurization and boiling) reportedly resembles that of volcanic eruptions, the difference recognized in the ground deformations is probably attributable to the different properties of magma and water. That is, temporal changes in ground deformations preceding explosions can be useful to understand internal or microscale processes of magma such as gas bubble growth and out-gassing.

Because the Vulcanian and Stromboli eruptions repeatedly occur at short time intervals, the conduit is considered an open system: the conduit is not closed, even if not filled with magma. Analyses of data from such repetitive explosions might be useful for understanding the magma dynamics because huge volumes of data can be obtained during a short observation period. For example, we can apply statistical tests to the data and examine models of magma migration in the conduit with high reliability. Therefore, in this study, relations of magma ascent in an open conduit to ground deformation are examined. We briefly explain the relation of ground deformation to magma ascent processes in an open conduit; subsequently, we formulate the ground deformation caused by magma in a narrow open conduit following Bonaccorso and Davis (1999). Temporal changes of ground deformation are affected by changes in both the strength and location of the pressure source in the conduit. Consequently, to elucidate relations of the basic process of magma ascent with ground deformation, we specifically examine three typical cases of magma ascent processes.

## 2. Source of ground deformation prior to intermittent volcanic eruptions from an open conduit

A schematic illustration of volcanic eruption from an open conduit is presented in Fig. 1. We presume that the volcanic conduit is connected to a deep magma chamber (not presented in Fig. 1) and that the magma

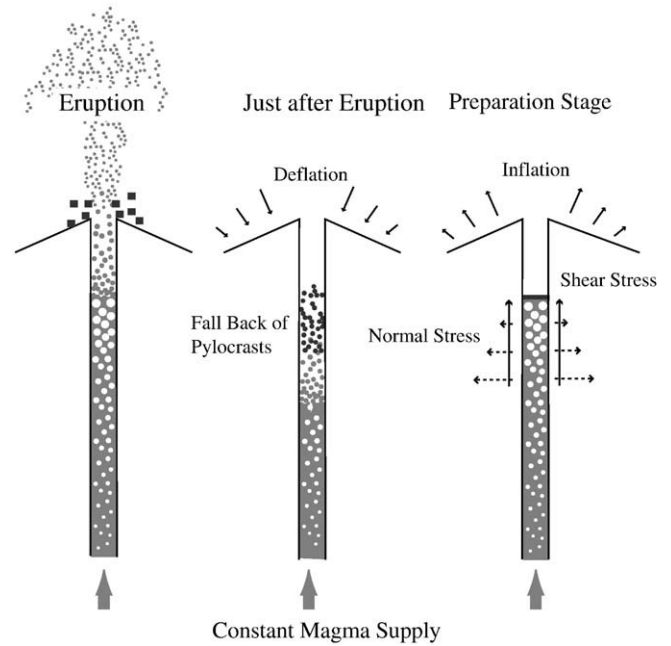


Fig. 1. Schematic illustration of eruption from an open conduit.

moves toward the shallow part of the conduit. Magma comprising viscous melt and numerous gas bubbles is considered to be supplied constantly from the deep magma chamber. Magma in the uppermost part of the conduit is ejected within a few tens of seconds to minutes. Then the magma remaining in the conduit is subjected to sudden depressurization because of the loss of magma when the eruption occurs. The pressure wave propagates downward with an acoustic speed to decrease the magma pressure in the conduit, when the magma viscosity is low and the conduit radius is large. Magma reservoir is depressurized by the loss of magma within a relatively short time, and the pressure drop in the reservoir may be almost the same to that in the conduit. Hence, new magma supply from deeper parts, where the depressurization due to the pressure wave caused by eruption is negligibly small, is necessary for producing the following eruption. On the other hand, when the magma viscosity is high and the conduit radius is small, the pressure wave propagation is not a dominant factor to reduce the magma pressure in the conduit. In this case, the magma pressure in the conduit gradually decreases due to viscous flow: magma starts to ascend at the top part in the conduit and then it propagates gradually into deeper parts. The viscous magma takes a sufficient time to balance the pressure difference between the top of conduit and deeper part. In the Appendix, the conditions producing the former and latter cases are quantitatively discussed by using a simple magma flow model.

Temporal and spatial changes of magma pressure are depicted schematically in Fig. 2. Magma fills the entire conduit immediately before eruption so that the magma pressure increases from a shallow part to a deep magma chamber. Once an eruption occurs, normal stress acting on the conduit wall decreases to the atmospheric pressure down to the depth of the magma head ( $z_{10}$  in Fig. 2). When the magma viscosity is low and the conduit radius is large, the magma reservoir pressure also decreases after the propagation of pressure waves triggered by a loss of magma at the top (Fig. 2b). When the magma viscosity is high and the conduit radius is small, the magma that is present at a deeper part ( $z > z_2$ ) is unaffected by the magma release (Fig. 2d). The depth  $z_2$  becomes deeper when the viscous flow effect is small (i.e., the pressure wave propagation becomes relatively dominant).

Volcano deflation is caused by these pressure decreases at the surface ground to that depth or to the reservoir. Then, as magma ascends gradually, the volcano starts to inflate because of the normal

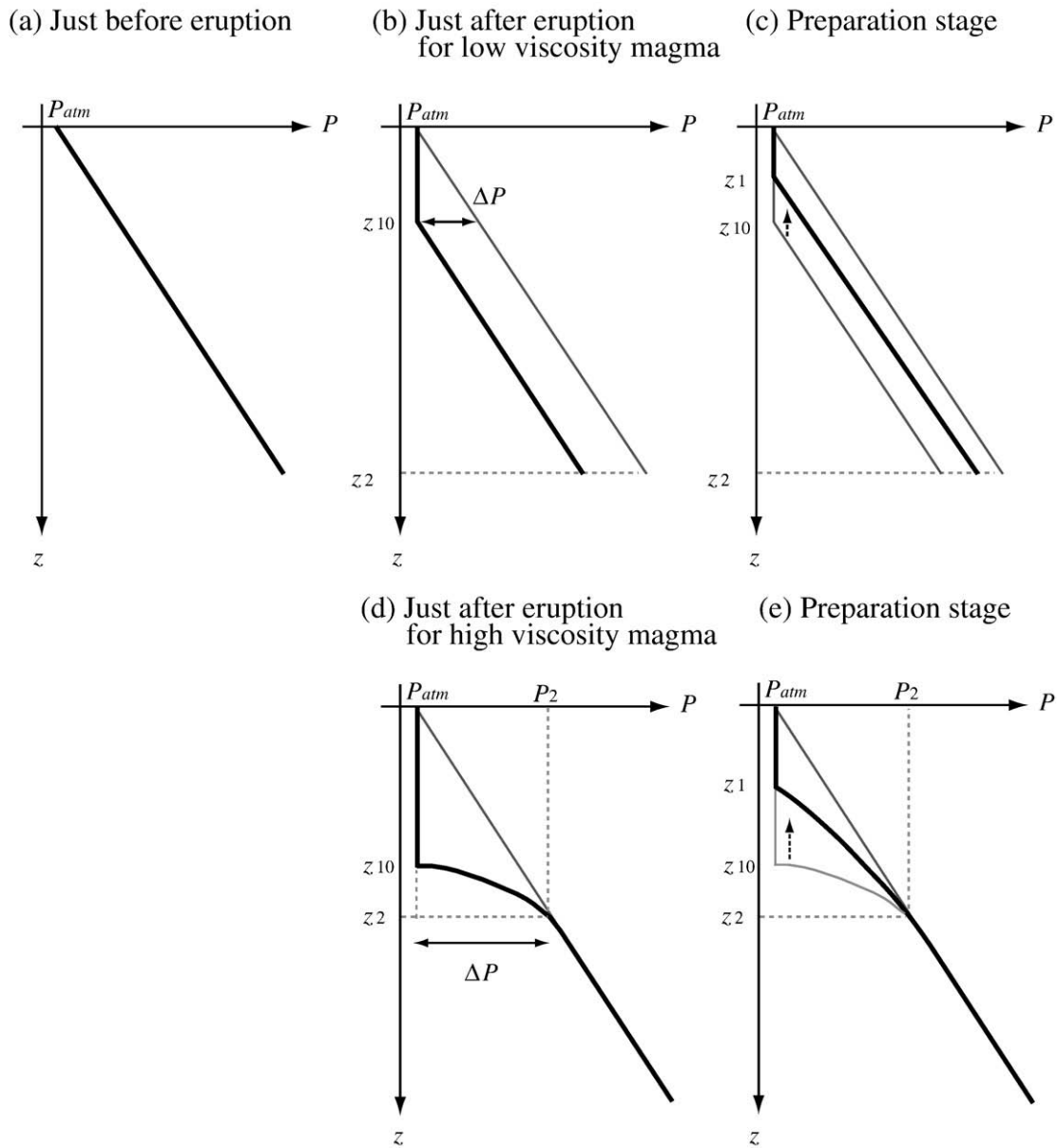


Fig. 2. Schematic illustration of spatio-temporal changes of magma pressure in an open conduit.

stress originating from magma pressure (Fig. 2c,e). Shear stress caused by a drag force associated with the motion of viscous magma might be another source for the ground deformation that is observed close to the vent (e.g., Chadwick et al., 1988; Beauducel et al., 2000; Green et al., 2006) when a counter force supporting the upward motion of magma is considered to be too deep to detect. Normal stress increases with depth because of gravitational force as well as pressure caused by shear stress, while shear stress is constant for depth when magma moves with a constant speed.

Several mechanisms can raise magma in the conduit. The first one is the supply of magma from a deep area, as driven by a pressure gradient generated by the removal of magma at the uppermost part of conduit. The second one is the gas bubble growth in magma associated with depressurization by eruption. Since the magma is subject to a sudden depressurization, the gas bubbles probably start to expand because of the pressure drop and diffusive mass transfer of water molecules from melt to gas bubbles. Such gas bubble growth can accompany the expansion of melt surrounding the bubbles. Therefore, magma migrates upwards in the open conduit. The last

mechanism is gas bubble rising in a low-viscosity melt. The gas bubbles can rise in the melt as a result of the buoyancy force when the melt viscosity is low and the rising gas bubbles are large. Because the ambient pressure decreases, their radii expand as they ascend. The total magma volume increases with time, pushing the magma that is above the bubbles upward in the conduit. These three magma behaviors are the main factors generating the normal and shear stresses on the conduit wall.

In the discussion presented in subsequent sections, we first relate the normal and shear stresses working on the conduit wall to the ground deformation. Then, the three mechanisms described above are modeled simply, with examination of their relations to ground deformation.

### 3. Ground deformation due to normal and shear stresses acting on the conduit wall

We first formulate the ground deformation attributable to the normal stress, following Bonaccorso and Davis (1999). We presume

that the cylindrical conduit extending along z-axis is deformed by the magma pressure,  $p(z)$ , and that the dislocation  $b(z)$  is normal to the vertically oriented cylinder wall. We obtain the radial displacement and vertical one  $u_z$  on the surface of a half-infinite medium, as

$$u_r = a \int_0^\infty b(z) \left( \frac{r}{R^3} - \frac{r}{2} \left( \frac{3z^2}{R^5} - \frac{2\nu}{R^3} \right) \right) dz$$

$$u_z = a \int_0^\infty b(z) \left( \frac{z}{R^3} - \frac{z}{2} \left( \frac{3z^2}{R^5} - \frac{2\nu}{R^3} \right) \right) dz, \tag{1}$$

where

$$b(z) = \frac{p(z)}{\mu} a,$$

and  $a$  is the radius of volcanic conduit,  $\nu$  is Poisson's ratio of the elastic medium,  $r$  is the distance from the exit of the cylindrical conduit (the origin of the coordinate) to the station,  $\mu$  is the rigidity of the elastic medium, and  $R = \sqrt{r^2 + z^2}$  (Fig. 3). Furthermore,  $u_r$  and  $u_z$  are positive, respectively, when the displacements are up and outward from the conduit. Herein, we assume that the conduit radius is sufficiently small compared with the distance from the conduit to a station (i.e.,  $a \ll r$ ).

Magma pressure at the shallow part of the conduit is expected to increase almost linearly with depth from the top of magma in the conduit. Consequently, we consider a case of vertical distribution of the magma pressure in the conduit, as shown below.

$$p(z) = \begin{cases} 0 & \text{at } 0 < z < c_1, c_2 < z \\ \frac{z-c_1}{c_2-c_1} \Delta P & \text{at } c_1 < z \leq c_2 \end{cases} \tag{2}$$

In that equation,  $\Delta P$  signifies the pressure difference at depths  $c_1$  and  $c_2$ . Note that we use symbols  $c_1$  and  $c_2$  instead of  $z_{10}$  or  $z_2$  shown in Fig. 2. The former symbols indicate the locations of the over pressure characterized by a shape of right-angle triangle, while the latter ones are used to represent the locations of the depressurization caused by eruptions. Substituting Green's function of the ground

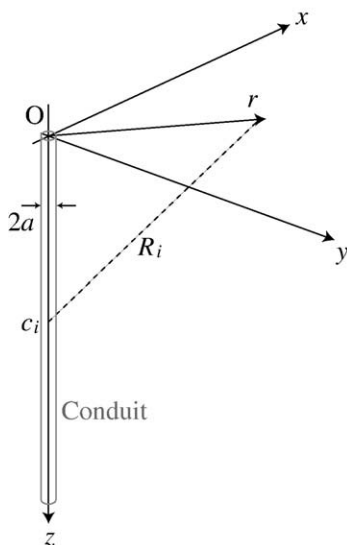


Fig. 3. Coordinate system of calculation.

surface at a distance of  $r$  from the vent into Eq. (1) and integrating it, we obtain the radial and vertical displacements as

$$u_r = \frac{mr}{c_2 - c_1} \left[ \frac{1}{2} \left( \frac{c_2^2}{R_2^3} - \frac{c_1^2}{R_1^3} \right) + \frac{c_1}{2r^2} \left( \frac{c_2^3}{R_2^3} - \frac{c_1^3}{R_1^3} \right) - \nu \left( \frac{1}{R_2} - \frac{1}{R_1} \right) - \frac{(1 + \nu)c_1}{r^2} \left( \frac{c_2}{R_2} - \frac{c_1}{R_1} \right) \right],$$

$$u_z = \frac{-m}{2(c_2 - c_1)} \left[ -\frac{c_2^2(c_2 - c_1)}{R_2^3} + (2\nu - 1) \left( \frac{c_2}{R_2} - \frac{c_1}{R_1} \right) - 2\nu c_1 \left( \frac{1}{R_2} - \frac{1}{R_1} \right) - (2\nu - 1) \ln \left( \frac{c_2 + R_2}{c_1 + R_1} \right) \right] \tag{3}$$

where  $R_i = \sqrt{r^2 + c_i^2}$  ( $i = 1, 2$ ) (Fig. 3) and  $m$  is the source strength represented as

$$m = \frac{\Delta P}{\mu} a^2. \tag{4}$$

The tilt is expressed as shown below.

$$\gamma = -\frac{\partial u_z}{\partial r} = \frac{mr}{2(c_2 - c_1)} \left[ \left( \frac{3c_2^2}{R_2^5} - \frac{2\nu}{R_2^3} \right) (c_2 - c_1) + \left( \frac{c_2}{R_2^3} - \frac{c_1}{R_1^3} \right) - (2\nu - 1) \left( \frac{1}{R_2(R_2 + c_2)} - \frac{1}{R_1(R_1 + c_1)} \right) \right] \tag{5}$$

Therein,  $\gamma$  is positive when the ground is up toward the vent.

Fig. 4 shows spatial changes of ground deformations caused by the normal stress for different heights of the top of the magma (i.e., magma head,  $c_1$ ). In the calculations, we normalize the variables relating distance or displacement by  $c_2$ , and those variables relating pressure by  $\mu$ . Normalized variables are indicated with a prime, such as  $u'_i, r', z'_i, R'_i, m'$ . The source strength of  $m' = 1$  is used in Fig. 4. The vertical displacements increase with distance from the conduit, reach maxima at a distance less than 1 ( $r' < 1$ ), then gradually decrease concomitantly with increasing distance. The distance  $r'$  showing the maximum amplitude decreases as the magma head  $c_1$  approaches the surface. Radial displacements and tilt exhibit spatial changes that are more complicated than those of the vertical displacement. Their amplitudes decrease concomitantly with increasing distance from the vent, and reach the minimum. The amplitudes increase, reach the maximum, and then gradually decrease with distance. The distances  $r'$ , showing the minimum and maximum amplitudes in these components, decrease concomitantly with increasing magma head height.

The ground deformation attributable to shear stress acting on the conduit wall can be approximated as a vertical single force when the conduit radius is small compared to the distance from the vent to stations. So, we present analytical expressions of ground deformation attributable to shear stress using the Boussinesque solution. We presume  $\tau$  to be the vertical single force acting on the circular conduit wall per unit area (i.e., shear stress). Then, the radial and vertical displacements, which tilt because of shear stress acting on the conduit wall at depths from  $c_1$  to  $c_2$ , are expressed as

$$u_r = sR \int_{c_1}^{c_2} \left( \frac{z}{R^3} - \frac{1-2\nu}{R(R+z)} \right) dz$$

$$= sr \left[ -\frac{1}{R_2} + \frac{1}{R_1} - (2\nu - 1) \left( \frac{1}{R_2 + c_2} - \frac{1}{R_1 + c_1} \right) \right] \tag{6}$$

$$u_z = s \int_{c_1}^{c_2} \left( \frac{z^2}{R^3} - \frac{2(1-\nu)}{R} \right) dz = s \left[ -\frac{c_2}{R_2} + \frac{c_1}{R_1} + (2\nu - 1) \ln \left( \frac{R_2 + c_2}{R_1 + c_1} \right) \right]$$

$$\gamma = s \int_{c_1}^{c_2} \left( -\frac{3z^2}{R^5} + \frac{2(1-\nu)}{R^3} \right) dz = \frac{s}{r} \left[ 2(1-\nu) \left( \frac{c_2}{R_2} - \frac{c_1}{R_1} \right) - \left( \frac{c_2^3}{R_2^3} - \frac{c_1^3}{R_1^3} \right) \right]$$

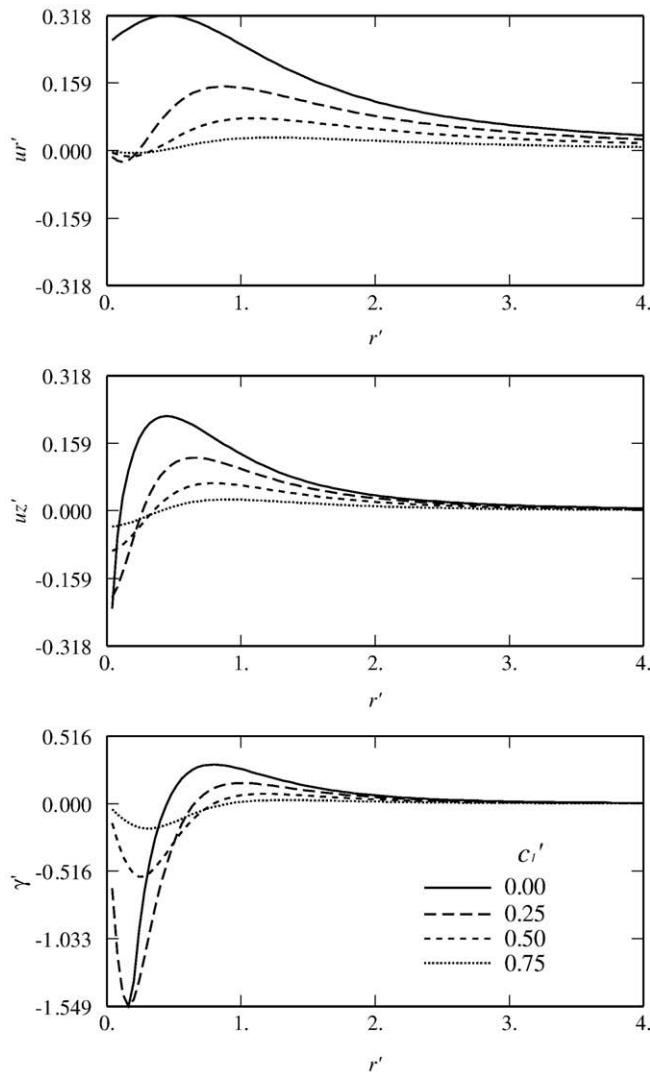


Fig. 4. Spatial variations of ground deformations caused by normal stress acting on the conduit wall at different depths.

where

$$s = \frac{\tau a}{2\mu} \tag{7}$$

Fig. 5 shows examples of spatial changes of deformations due to shear stress for different magma head heights. The variables are normalized, as they are in the case of normal stress. The displacements and tilt are calculated for  $s' = \tau a' / 2 = 1$ . Amplitudes of vertical displacements are larger than the horizontal displacements: the maximum displacements appear at distances less than the magma depth ( $r' < 1$ ). The distances  $r'$  where the maximum amplitudes of vertical displacements are observed decrease as the magma head  $c_1'$  approaches the surface. Radial displacements and tilt show negative values close to the vent, and gradually increase concomitantly with increasing distance, except  $c_1' = 0$ . The distances at which the minimum and maximum amplitudes are observed to decrease concomitantly with increasing position of the magma head.

Some components diverge at  $r' = 0$ , as shown in Figs. 4 and 5. In Eq. (1), the displacement field is derived from the Green's function for a uniform elastic half-space in which no cylindrical surface is considered. Therefore, we are unable to discuss the displacement field behavior very close to the vent.

These results indicate that magma locations in the conduit change the spatial variations of ground deformations. Alternatively, depths of  $c_1$  and  $c_2$  can be determined from spatial variations of horizontal and vertical displacements and tilt records. In addition, because spatial variations of the deformations mutually differ according to normal and shear stresses, measurements of ground deformation at many sites on the volcano enable us to estimate the contribution of the strengths of normal stress source  $m$  and single force  $s$ .

#### 4. Ground deformation due to ascent of magma without gas bubble growth

We first examine the magma motion and ground deformation for the ascent of magma that does not accompany gas bubble growth. Such magma might not generate an explosion at the surface, but this example is a good reference for understanding the ground deformation caused by magma migration in the conduit. We simplify the magma motion in the conduit as follows (Fig. 6). The magma head pressure at a depth  $z_1$  is always equal to the atmospheric pressure  $P_{atm}$ . The magma at depths greater than  $z_2$  is unaffected by eruptions; the magma pressure at that depth is designated as  $P_2$ . This is the case of Fig. 2d and e: the conduit is mainly depressurized by the viscous flow in a narrow conduit. The case of Fig. 2b and c is discussed later in this subsection. The magma head locates initially at a depth of  $z_{10}$ ; then it ascends because of a pressure gradient that is formed in the magma at

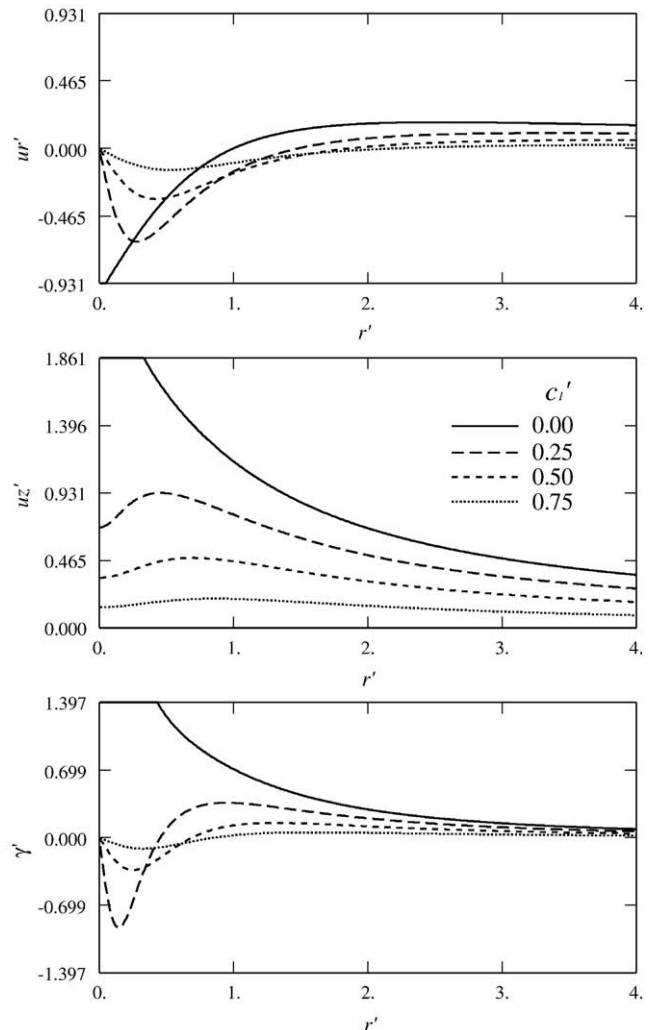


Fig. 5. Spatial variation of ground deformations caused by shear stress acting on conduit wall at different depths.

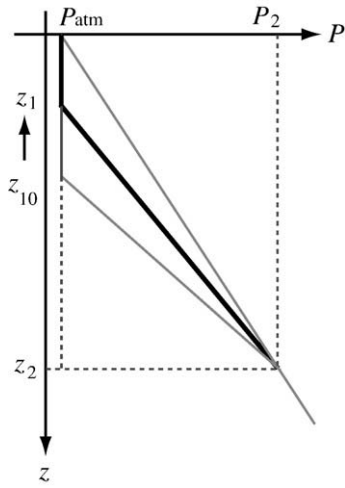


Fig. 6. Schematic illustration of temporal changes of magma pressure for magma without gas bubble growth.

$z_1-z_2$ . Magma ascent without gas bubble growth (i.e., no change in bubble volume) is approximated as a Poiseuille flow in a circular pipe. As a simplification, we designate the pressure gradient at depths  $z_1-z_2$  as approximately linear. Consequently, the magma head depth  $z_1$  is expressible as

$$\frac{dz_1}{dt} \cong -\frac{a^2}{8\eta z_2-z_1} \frac{\Delta P}{\rho g} + \rho g, \tag{8}$$

where  $\Delta P = P_2 - P_{atm}$ ,  $\eta$  is the melt viscosity,  $\rho$  is the magma density, and  $g$  is the gravitational acceleration. Solving Eq. (8), we obtain

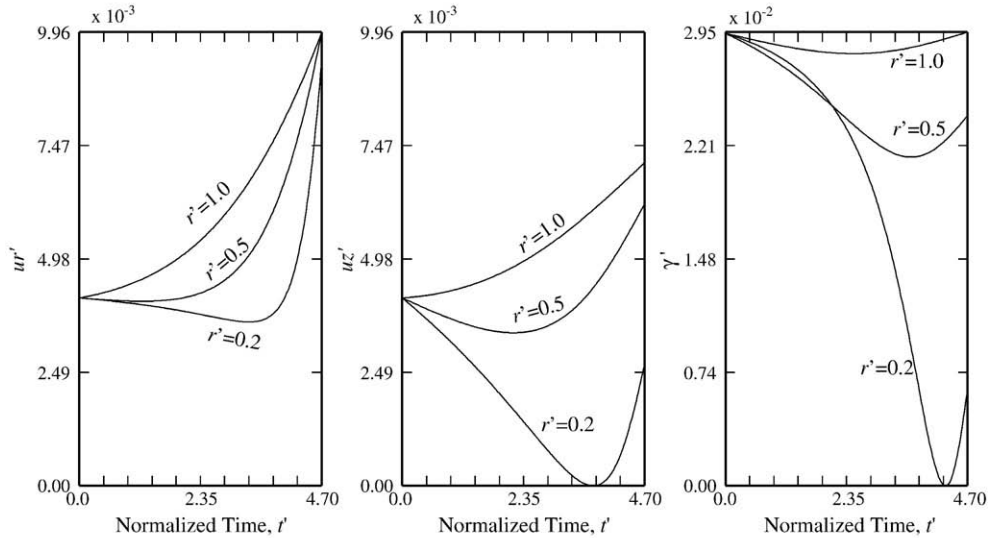
$$t' = (z_1'-1) - \alpha_p \log \left| \frac{\alpha_p - (z_2' - z_1')}{\alpha_p - (z_2' - 1)} \right|, \tag{9}$$

where  $t' = t/\tau_p$  and

$$\tau_p \equiv \frac{8\eta z_{10}}{\rho g a^2}, \alpha_p \equiv \frac{\Delta P}{\rho g z_{10}}. \tag{10}$$

Normal Stress, No Bubble Growth:  $z_2=50, z_{10}=1, \alpha_p=60$

Near Field



Far Field

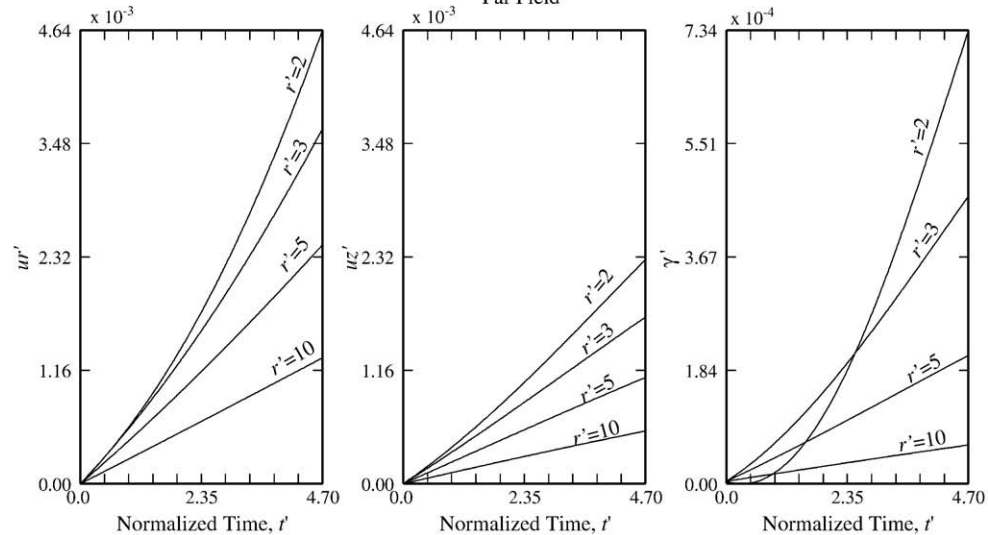


Fig. 7. Temporal changes of ground deformation attributable to normal stress caused by the ascent of magma without gas bubble growth for the case of  $z_2=50, z_{10}=1$ , and  $\alpha_p=60$ .

Variables relating to the distances are normalized by  $z_{10}$ . The solution indicates that low-viscosity magma can rise fast in a wide conduit (see Eq. (10)) and that the migration speed is greatest at the beginning and gradually decreases with time. Hence,  $s$  for the shear stress changes with the magma head depth.

$$s = \frac{a^2}{4\mu} \left( \frac{\Delta P}{z_2 - z_1} - \rho g \right) = \frac{m}{4z_{10}} \left( \frac{1}{z_2 - z_1} - \frac{1}{\alpha_p} \right). \quad (11)$$

On the other hand, the source term  $m$  for the normal stress is constant. Ground deformations of radial and vertical displacements and tilt caused by normal and shear stresses are calculated from Eqs. (3)–(6) and (9)–(11).

Fig. 7 presents temporal changes of the ground deformation caused by the normal stress for  $m' = 1$  and  $\alpha_p = 60$ . The time is normalized by  $\tau_p$ , and the calculation is truncated when  $z_1' = 0.001$ . Ground displacements and tilt at locations close to the vent ( $r' \leq 1$ , hereinafter near field) show a slightly complicated change with time, reversing their polarities. At far fields of  $r' > 1$ , the temporal changes are simple: radial and vertical displacements respectively indicate

continuous outward and upward movements. Tilt is up toward the vent. These changes are almost proportional to  $t$ . In the case of smaller  $\alpha_p$ , however, the ascent speed of magma level decreases because the pressure gradient decreases with increasing time. For that reason, the rates of changes in ground deformation decrease with time.

Fig. 8 shows the ground deformations due to shear stress for  $m' = 1$  and  $\alpha_p = 60$ . The characteristics of temporal changes in the displacements and tilt are similar to those due to normal stress: complicated behavior at near field and constant changes at the far field. The vertical displacements at far fields ( $r' > 5$ ) reflect ground subsidence resulting from the slowing ascent of magma in the conduit.

Eq. (11) relates the strength of the source terms of normal and shear stresses, which enables us to determine the contributions of the two kinds of stress to the ground displacement. For example, at  $r' = 2$ , the amplitude of vertical displacement caused by normal stress is about six times larger than that by shear stress (see Figs. 7 and 8). Fig. 9 plots the ground deformations caused by both normal and shear stresses. It is found that the overall characteristic of temporal changes is similar to the case of the ground deformation caused by normal stress (Fig. 7).

When the magma viscosity is low and the conduit is wide (the case of Fig. 2b and c), the magma comes to be supplied from deeper parts. Hence,

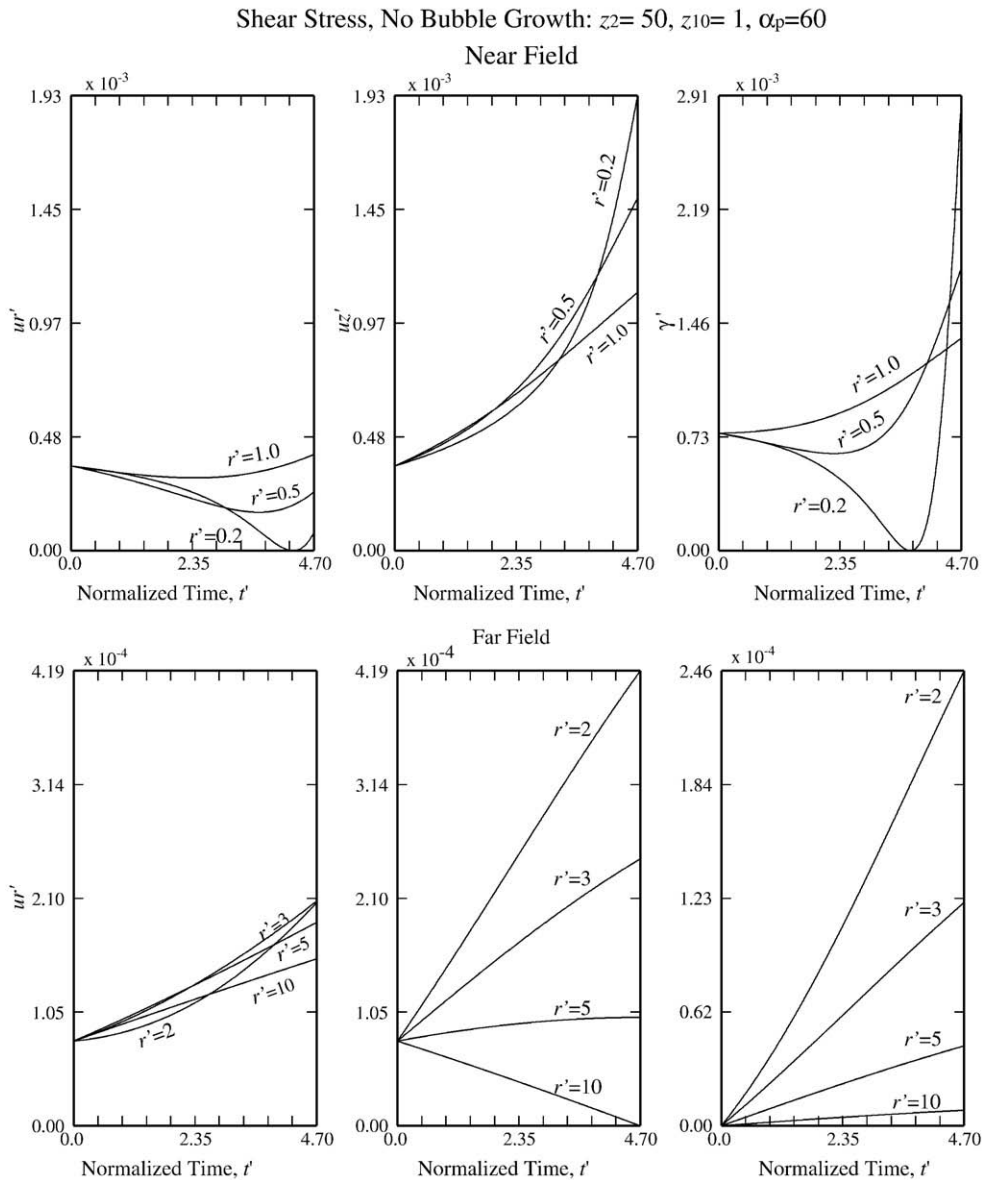


Fig. 8. Temporal changes of ground deformation attributable to shear stress caused by the ascent of magma without gas bubble growth for the case of  $z_2 = 50, z_{10} = 1$ , and  $\alpha_p = 60$ .

Normal and Shear Stresses, No Bubble Growth:  $z_2=50, z_{10}=1, \alpha_p=60$

Near Field

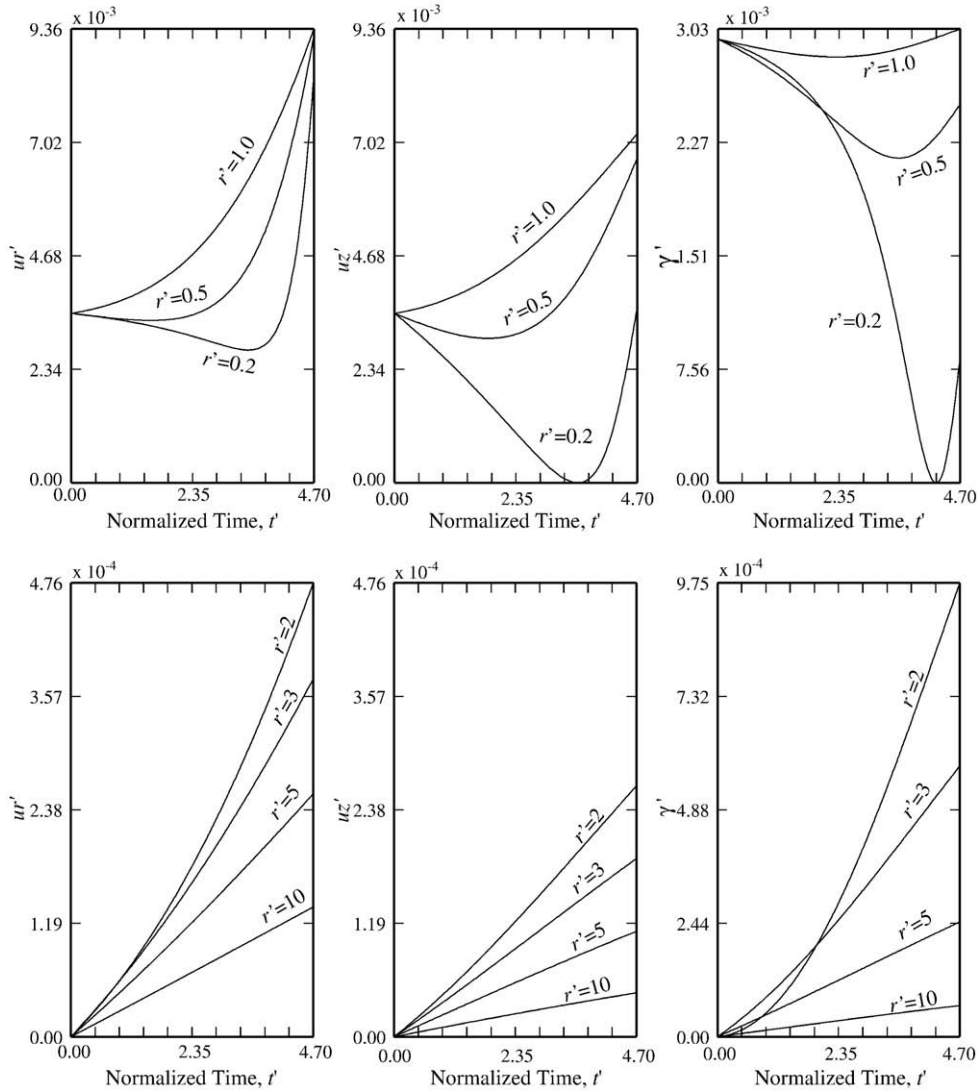


Fig. 9. Temporal changes of ground deformation attributable to both normal and shear stresses caused by the ascent of magma without gas bubble growth for the case of  $z_2 = 50$ ,  $z_{10} = 1$ , and  $\alpha_p = 10$ .

more complicated boundary condition is necessary. If the magma is constantly supplied from the deep parts, the magma in the conduit will migrate upward with a constant speed. In such case, the ground deformations would be similar to the results shown in Figs. 7, 8 and 9, because large  $\alpha_p$  makes the magma upward migration speed almost constant.

5. Ground deformation due to magma with gas bubble growth by diffusive process

Rapid depressurization occurring in the uppermost part of the magma in the conduit immediately after eruptions can trigger gas bubble growth in magma. The magma volume expands so that the free-surface level rises in the conduit. In this section, we simplify this process by considering the gas bubble growth caused by the diffusion mass transfer of water molecules from the bulk of the supersaturated melt to the bubble–melt interface. We describe its relation to the ground deformation. Fig. 10 presents a schematic illustration of the model of magma ascent in an open conduit. The magma within the conduit, which contains numerous gas bubbles in the melt, is subject to sudden depressurization with amplitude of  $\Delta P$  (for the case of Fig. 2d, the amplitude is estimated to be  $(P_2 - P_{atm})z_{10}/(2z_2)$  on

average) immediately after eruptions. The top layer of magma, whose height is  $h_0 = z_2 - z_{10}$ , starts to expand its volume because of gas bubble growth driven by the diffusion mass transfer.

We first estimate the volume changes of magma; then we evaluate the ground deformation that is attributable to them. Gas bubble growth behaviors are fundamentally expressed by the equation of motion of melt at the boundary of the melt and gas, a diffusion equation of  $H_2O$  molecules in the melt, the equation of mass conservation of  $H_2O$  in the gas bubbles, the equation of a perfect gas, and the equation of pressure balance between the magma and the surrounding medium (Shimomura et al., 2006). Concentration of  $H_2O$  at the gas–melt boundary obeys Henry’s law. Exact solutions of the gas bubble growth are obtained by calculating these fundamental equations numerically for various settings. However, analytical solutions in some simple cases elucidate the physical parameters that control the ground deformation.

The Peclet number,  $Pe$ , is often used to indicate how gas bubbles expand in magma that is subject to a sudden decompression. The Peclet number can be expressed as (e.g., Lyakhovskiy et al., 1996)

$$Pe = \frac{\Delta P R_g^2}{\eta D}, \tag{12}$$

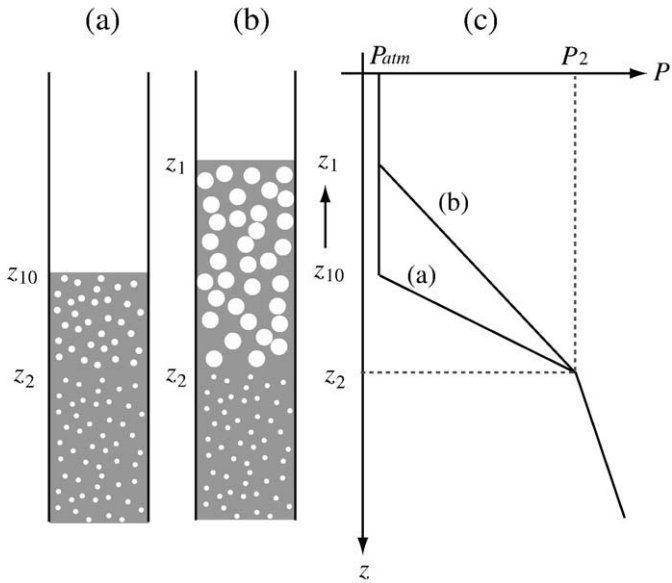


**Fig. 10.** Model of ascent for gas-bubble-containing magma in an open conduit. The gas bubbles in magma expand by diffusion mass transfer of water molecules.

where  $R_g$  represents the gas bubble radius and  $D$  is the volatile diffusivity in the melt. Diffusion mass transfer is dominant in the bubble growth process for small  $Pe$  ( $< 1$ ), whereas the growth is controlled by viscous expansion for  $Pe \gg 1$ .

We might estimate  $Pe$  from observations and simple consideration. First, consider the case of the Stromboli volcano as an example of basaltic magma. The magma volume for each small explosion is estimated at  $0.5\text{--}2.4\text{ m}^3$  (Harris and Ripepe, 2007). Hence, the thickness of magma effused by one eruption is estimated at  $0.2\text{--}0.8\text{ m}$  for a conduit radius of  $1\text{ m}$ . Assuming the magma density to be  $1000\text{ kg/m}^3$  (Lautze and Houghton, 2007), we estimate  $\Delta P$  to be  $1 \times 10^4\text{ Pa}$ . For  $D$  of  $10^{-8}\text{ m}^2/\text{s}$ ,  $\eta$  of  $10^2\text{ Pa s}$  and  $R_g$  of  $1\text{ mm}$ ,  $Pe$  is estimated to be about  $10^4$ . For a high-viscosity magma such as rhyolite, we might use the following typical values:  $\eta = 10^6\text{ Pa s}$ ,  $D = 10^{-11}\text{ m}^2/\text{s}$ . In such a case,  $R_g$  and  $\Delta P$  might be distributed in a wide range, but presuming  $R_g$  of  $10^{-5}\text{ m}$  and  $\Delta P$  of  $0.1\text{ MPa}$ , we obtain  $Pe$  of about  $1$ . These estimations suggest that the bubble growth process might be expressible by viscous expansion when the magma is depressurized suddenly by eruption.

However, such a large Peclet number might immediately approach a small value. As an extreme case, we consider that the bubble growth is controlled by the equation of motion and that no diffusion mass transfer occurs between the melt and gas bubbles. When the gas bubbles are depressurized suddenly from  $P_0$  to  $P_f$ , the gas density,  $\rho_g$ , in bubbles follows the equation

$$\rho_g^{-1}(t) = \rho_{gf}^{-1} + (\rho_{g0}^{-1} - \rho_{gf}^{-1})e^{-\frac{3P_f}{4\eta}t}, \quad (13)$$

where  $\rho_{g0}$  and  $\rho_{gf}$  respectively signify the gas density at the initial and final conditions. This result indicates that gas density  $\rho_g$  does not change so much after a characteristic time:  $4\eta/3P_f$ . That characteristic time is estimated as much less than a second for basaltic magma and as a few seconds for rhyolite magma, assuming  $P_f$  of atmospheric pressure. The estimation suggests that a few seconds after the sudden depressurization, then  $d\rho_g/dt \rightarrow 0$  and  $Pe < 1$ . We assume that the gas bubble growth in magma at the uppermost part of conduit can be expressed approximately by the diffusion mass transfer during the most preparation stages of magma ascent before an eruption.

When gas bubbles in the melt are small and their separations are approximated as infinite, the gas bubble radius resulting from the

diffusion mass transfer is expressed analytically as (Lyakhovskiy et al., 1996)

$$R_g^2(t) = \frac{2D\rho_l(C_0 - C_f)}{\rho_g}t, \quad (14)$$

where  $\rho_l$  is the melt density, and  $C_0$  and  $C_f$  denote the initial and final water concentration in the melt, respectively. Introducing the gas bubble number density  $n_g$ , we obtain the height of the magma column as

$$h(t) = h_0 \left( 1 + \left( \frac{t}{\tau_d} \right)^{1.5} \right), \quad (15)$$

where

$$\tau_d \equiv \left[ 2n_g^{2/3} D \frac{\rho_l}{\rho_g} (C_0 - C_f) \right]^{-1}. \quad (16)$$

Characteristic time  $\tau_d$  becomes small for the magma highly vesiculated and/or having large diffusion coefficient. The bulk density and velocity of magma are

$$\rho(t) = \frac{\rho_l}{1 + (t/\tau_d)^{1.5}} \quad (17)$$

and

$$v_m(t) = \frac{\dot{h}(t)}{2} = \frac{3h_0}{2} \left( \frac{t}{\tau_d} \right)^{0.5}. \quad (18)$$

Fig. 11 presents examples of temporal changes of ground deformation by normal stress. Similarly to the magma without gas bubble growth, the ground deformations observed at near field ( $r' \leq 1$ ) turn their polarities during the magma ascent. On the other hand, the ground deformation at a far field ( $r' > 1$ ) is simple: amplitudes of the displacements and tilt increase with time. The rates of change are recognized to increase with time because the graphs of Fig. 11 depict concave shapes. The ground deformations in radial and vertical displacements and tilt are proportional to  $t^{1.5}$  in a far field.

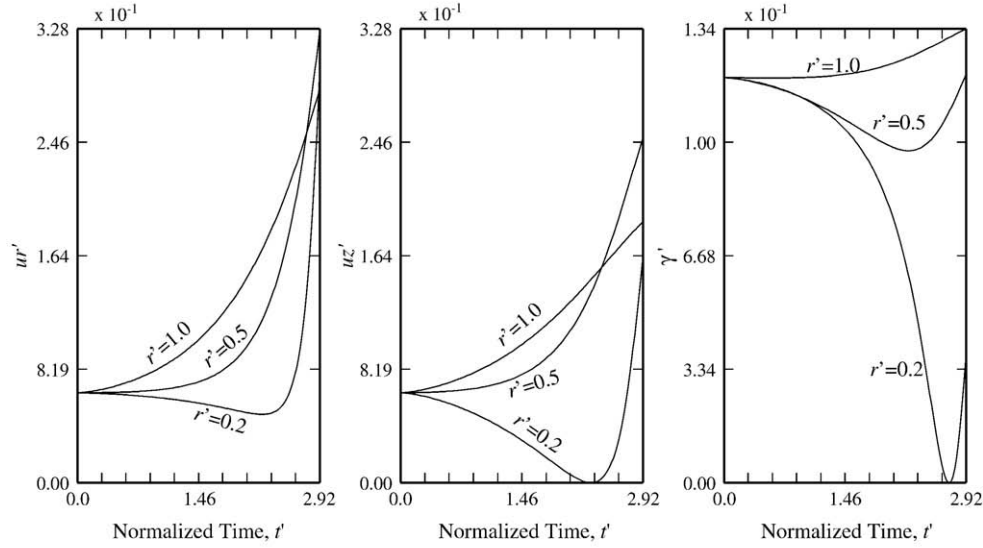
Shear stress resulting from the magma motion according to the gas bubble growth must be exerted on the conduit wall. We may obtain a relation between the strengths of normal and shear stresses, similarly to Eq. (11) if the shear stress is proportional to the magma velocity, similarly to a Poiseuille flow. However, for a more quantitative discussion, it might be necessary to clarify the generation of viscous drag force on the conduit when the magma expands in the conduit because of gas bubble growth.

When the viscous effect is large in the conduit (Fig. 2d), the pressure drop given at the uppermost part of the conduit might not be constant: the pressure drop amplitude probably decreases concomitantly with increasing depth (see Fig. 2d). Such vertical changes in the pressure drop might not be expressed completely by the bubble growth process described above, in which only the behavior of gas bubbles subjected to a constant pressure drop is examined. However, even such vertical variation exists in pressure: the gas bubble growth process can obey the diffusion mass transfer at each depth. Therefore, the rate of ground deformation ( $\propto t^{1.5}$ ) is inferred to be the same as that in the case of a constant pressure drop.

These formulations are derived based on the assumption that the radius of each gas bubble is much smaller than the radius of the melt surrounding the bubble (Lyakhovskiy et al., 1996). The growth rate decreases and converges to zero as the melt and gas bubbles approach equilibrium when the gas bubbles expand (Prousevitch et al., 1993; Shimomura et al., 2006). Inflatons of the conduit cease before eruptions if eruptions do not occur before such an equilibrium is attained.

Normal Stress, Bubble Growth:  $z_2=1.2$   $z_{10}= 1.0$

Near Field



Far Field

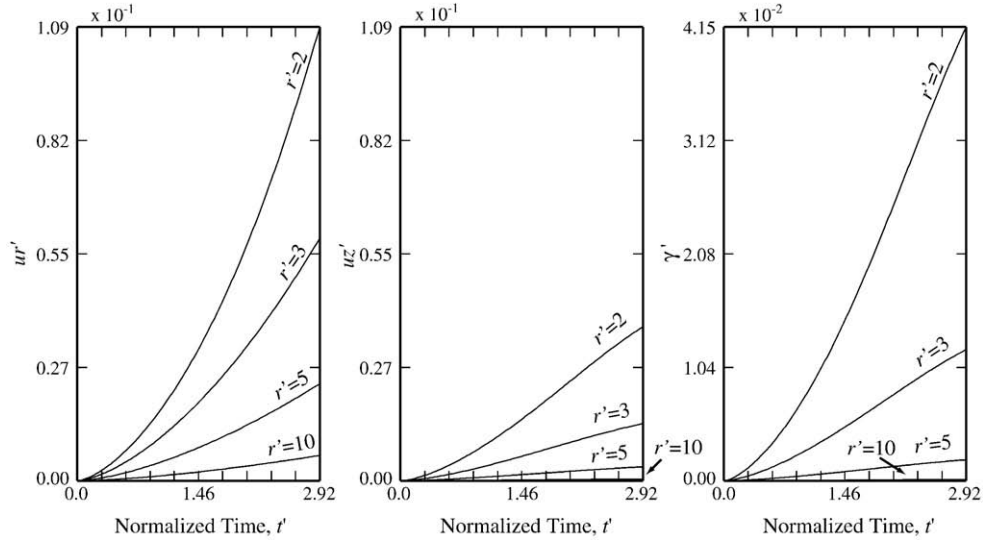


Fig. 11. Temporal changes of ground deformation at near and far fields attributable to normal stress caused by magma ascent as a result of diffusion mass transfer. The magma was located initially from  $z_2=2.0$  to  $z_1=1.0$ .

6. Ground deformation due to gas bubbles rising in magma

Gas bubbles can migrate upward in the melt with low-viscosity magma and large gas bubbles. The gas bubble expansion can be introduced by a decrease of the surrounding pressure instead of by diffusive transfer of volatiles from the melt. The Peclet number for such a condition is large ( $Pe > 1$ ) if the velocity is sufficiently high.

We consider that gas bubbles in magma are distributed non-uniformly in the conduit and that, in some regions, large gas bubbles group together. Such a situation might occur because the rise of a large gas slug is used to interpret the mechanisms of explosions at Stromboli volcano (Jaupart and Vergnolle, 1988); moreover, gas bubbles apparently concentrate in some layers during ascent even if they are initially distributed uniformly (Manga, 1996). To simplify the model, the present study does not incorporate bubble coalescence in the following.

When gas bubbles ascend in the melt, they occupy the upper melt space. The melt must descend to fill the empty space where the gas bubbles reside before rising. However, because the gas bubble volume increases as a result of the pressure decrease induced by the rise, some

of the melt will move somewhere else. Compressibility of magma is low in deeper areas in the conduit. For that reason, the melt is inferred to move upward more easily, pushing upward to the magma free-surface level. Such a process continues during the gas bubbles' ascent; the magma level rises continuously to the surface over time. Sudden depressurization of magma accompanied with the previous eruptions is not related directly to the behavior of rising gas bubbles; that intermittency of eruptions is controlled by vertical distributions of the rising gas bubbles.

First, we examine the volume expansion of the gas bubbles resulting from depressurization associated with the gas bubble ascent in the melt. Applying principles of Stokes' flow, we express the gas bubble velocity as

$$\frac{dz_g}{dt} = -\frac{R_g^2(t)}{3\eta}(\rho_l - \rho_g(t))g, \tag{19}$$

where  $z_g$  represents the gas bubble depth. Here, the gas bubble radius is much smaller than the conduit radius. Assuming that the gas in the

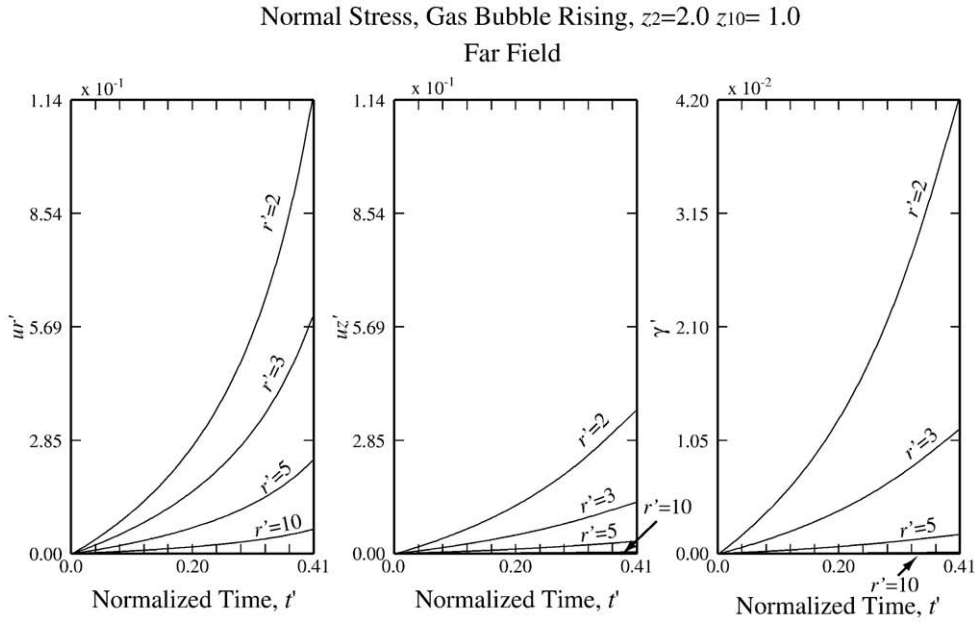


Fig. 12. Temporal changes of ground deformation at far fields attributable to normal stress caused by magma ascent as a result of rising gas bubbles.

bubbles follow the equation of a perfect gas and assuming that the mass transfer between the bubble–melt interfaces is negligible, we obtain

$$p_g \rho_g^{-1} = p_{g0} \rho_{g0}^{-1}, \tag{20}$$

where subscript 0 on the right side of the equation represents the initial value when the gas bubbles start to rise. The gas bubble pressure can be related to the speed of a spherical gas bubble's rise.

$$\frac{dp_g}{dt} = \rho_g g \frac{dz_g}{dt} \tag{21}$$

We consider that  $N_g$  gas bubbles having the same bubble radius migrate upward similarly in the melt; therefore, the total gas bubble volume is expressed as  $V = 4\pi N_g R_g^3 / 3$ . Normalizing the parameters in Eqs. (19)–(21) using the relations of

$$V' = V / V_0, \rho'_{g0} = \rho_{g0} / \rho_l, t' = t / \tau_r, \tag{22}$$

where  $V_0$  is the initial gas bubble volume and

$$\tau_r \equiv \frac{3\eta z_{g0}}{\rho_l g r_{g0}^2}, \tag{23}$$

we obtain

$$\frac{dV'}{dt'} = V'^{\frac{5}{3}} (V' - \rho'_{g0}). \tag{24}$$

In a shallow region, the initial gas density is estimated at less than one-tenth or one-hundredth of the melt density. Therefore, neglecting the term of  $\rho'_{g0}$  in Eq. (24), we obtain the following solution.

$$V' \cong \left(1 - \frac{5}{3} t'\right)^{-\frac{3}{2}} \tag{25}$$

Eq. (25) represents that gas bubbles slowly increase their volume initially, then gradually increase the rate of volume expansion with time, and finally diverge at a time of  $t' = 3/5$ . The lapse time of gas bubble rising becomes longer as the initial gas bubble radius becomes smaller and/or as the magma viscosity increases (see Eq. (23)). Fig. 12

shows temporal changes of ground deformations for the normal stresses in the far fields. For this calculation, we presume that the rising bubble is always below  $z_2$  and that magma that is present above the bubbles is lifted by the volume expansion of ascending gas bubbles. The pressure at  $z_2$  increases with time. For that reason, we substitute  $m' = 1 + z_2 - z_1$  into Eqs. (3)–(5). The calculation is truncated at a time of  $t' = 0.41$ , when the magma level in the conduit reaches the ground surface. Fig. 12 clarifies the degree to which the deformations accelerate with time.

The source area in which shear stress operates is assumed to be the magma above the bubbles. However, because no constraint is given in the locations of magma in the conduit for the present simple model, the contribution of a single force is not discussed.

### 7. Discussion

Three different models of magma ascent in an open conduit were investigated through examination of their respective relations to ground deformation. The simple models elucidate some important aspects of the relation of volatile behavior in magma to ground deformation. As has been estimated already at many active volcanoes, the source depths (e.g.,  $z_1$  and  $z_2$ ) can be estimated using spatial distributions of horizontal and vertical displacements and/or tilt records. Sources of two kinds—normal and shear stresses—are estimated from the data of dense geodetic networks deployed around the conduit. Amplitudes of the deformations are also used to estimate the source strength,  $m$  and  $s$  in Eqs. (4) and (7), which might be related to the density and viscosity of magma, and the conduit radius.

The characteristics of temporal changes in the ground deformations can constrain the mechanisms of magma's ascent in an open conduit. Vertical displacements at far fields for the three different mechanisms are compared in Fig. 13 using a logarithmic scale. The time on the horizontal axis is normalized by the lapse time,  $t_{max}$ , during which the magma head residing at  $z_{10}$  reaches the ground surface ( $z = 0$ ), and displacements are normalized by the maximum value in the displacements that are shown. It is plausible that magma migration does not accompany gas bubble growth when the observed ground deformation is proportional to time at far fields or when the rate of change in deformation decreases with time (Fig. 13a). Ground deformations that are proportional to the 1.5 power of time suggest magma ascent with gas bubble growth caused by the diffusion mass

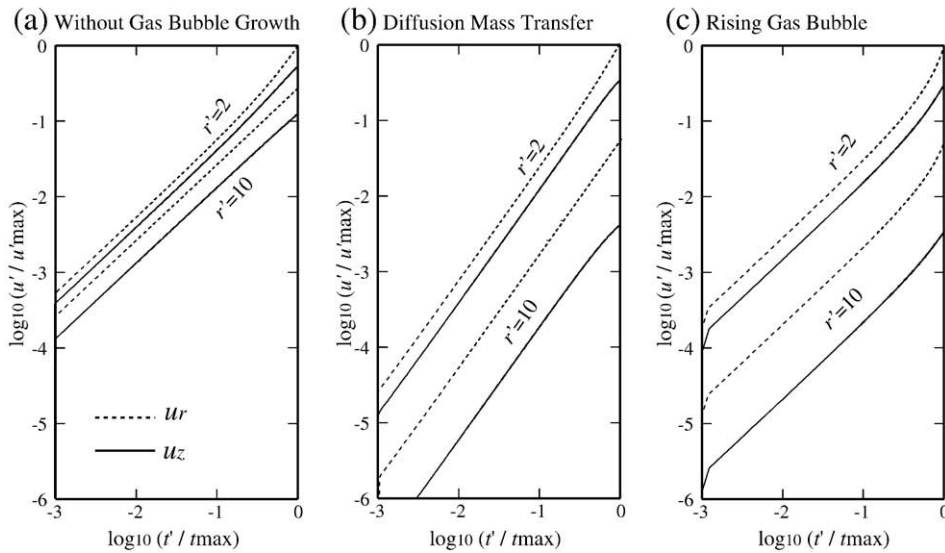


**Fig. 13.** Comparison of vertical displacements caused by (a) magma ascent without gas bubble growth, (b) magma ascent with gas bubble growth because of diffusion mass transfer, and (c) magma ascent because of rising gas bubbles, as plotted on logarithmic scales.

transfer of water molecules in the melt (Fig. 13b). Gas bubble ascent in the melt might occur in the conduit when a rapid increase of the rate of temporal change of ground deformation precedes basaltic magma eruptions (Fig. 13c). These differences strongly suggest that the temporal changes in ground deformation reflect the mechanism mainly controlling the magma ascent.

The characteristic times ( $\tau_p, \tau_d$ , and  $\tau_r$ ) of the models, which characterize the physical parameters controlling the duration of the magma ascent, can be estimated from the interval times of successive eruptions as well as other parameters described above (e.g.,  $z_1, z_2, a$ ). The characteristic time  $\tau_p$  is in the range of a few seconds to a few hundred minutes for the magma with  $\eta$  of  $10^2$ – $10^5$  Pa s in the conduit of  $a = 2$  m and  $z_{10} = 1000$  m. Since the initial depth of magma head can be estimated from the spatial distributions of volcano inflation, we are able to evaluate the ratio of  $\eta / (\rho a^2)$ , which represents the viscous effect in magma motion in the conduit. Regarding the magma ascent attributable to diffusion mass transfer, the diffusion parameter  $n_g^{2/3} D$  (Mason et al., 2006) may be estimated from Eq. (16) by substituting the appropriate density of the melt and gas, and the concentration of volatiles. This is an important parameter that is related to the eruption duration, which may be in the range of about  $10^{-6}$  s $^{-1}$  to  $0.5$  s $^{-1}$  (Mason et al., 2006). For magma having the melt density of  $2000$  kg/m $^3$ , the gas density of  $20$  kg/m $^3$ , and  $C_0 - C_f$  of  $0.01$ ,  $\tau_d$  is estimated to be from  $10$  min to  $1$  s. Ground deformation data due to the magma ascent by rising gas bubbles might enable us to estimate the ratio of the initial gas bubble radius and the depth at which gas bubbles start to rise in the conduit, as well as the total number of gas bubbles. For  $\rho_l = 2000$  kg/m $^3$ ,  $\eta = 10^2$  Pa s,  $z_{g0} = 100$  m, and  $r_{g0}$  of  $0.1$ – $0.01$  m,  $\tau_r$  is estimated to be from  $2.5$  min to  $250$  min. That is,  $t_{\max}$  are estimated to be about  $1$  min to  $100$  min, which are in the range of interval times of repetitive eruptions observed at active volcanoes. However, it is necessary for this model to explain the relations of the rising gas bubble process to, for example, timings of eruptions and the repeatability and mechanisms of explosions.

Some previous studies presumed the existence of a cap of some kind at the top of the magma in the conduit to generate explosion earthquakes that are often observed in association with Vulcanian and Strombolian eruptions (e.g., Ishihara, 1985; Nishimura and Chouet, 2003; Tameguri et al., 2002; Ohminato et al., 2006). It is not well known how such a 'cap' is formed at the top of magma head or in the bottom of crater, but it might result from, for example, a combination of falling back of pyroclasts into the conduit after eruptions,

successive degassing that raises the melt viscosity, and solidification of magma through cooling. The magma might be pressurized during its ascent because of viscous drag or friction between the cap and surrounding rocks if such a cap is formed at the top of magma in the conduit. These magma pressurizations restrict gas bubble expansion in the magma. Shimomura et al. (2006) numerically simulated the gas-bubble growth process in magma surrounded by elastics. The rate of change in the gas bubble radius is explained by diffusive growth when the elastic effect is negligibly small (i.e., the radius increases in direct relation to the root of time). However, the rate decreases as the elastic effect becomes large. Their results suggest that formation of a 'cap' or high-viscosity layer at the top of the magma in the conduit can decrease the gas-bubble expansion rate and temporal changes in ground deformation.

Magma migrations in actual active volcanoes cannot be approximated by one of the three models. For example, repeated eruptions require the constant addition of new magma from a deeper region. Consequently, ground deformations are caused by such additional sources and by others such as bubble growth. Although this study specifically examined investigating the characteristics of ground deformation generated by each basic process of magma migration, a better quantitative comparison can be made by numerically calculating the melt motion as well as the gas bubble expansion and motion based on the fundamental equations controlling their behavior. Through such numerical calculations, we are further able to incorporate some important aspects of magma properties, such as degassing and crystallization, which engender spatial changes of density and viscosity of magma in the conduit.

Figs. 4 and 5 in Iguchi et al. (2008) might be useful to examine the characteristics of temporal changes in ground deformations observed at active volcanoes. Because we must confront difficulty or ambiguity in measurements of the start and end times of each eruption from these figures, we are unable to measure the ground deformation rate. However, increases in the rates of the deformation prior to explosions strongly suggest the existence of bubble growth processes in the conduit. Additional observations of ground deformation and measurements of the start and stop times of each eruption can provide important constraints on the conduit processes occurring prior to volcanic explosions. When we compare such field observations with results from numerical simulations, it is also necessary to evaluate the effects of topography of the target volcano precisely, using, for example, finite element methods or boundary element methods (e.g.,

Cayol and Cornet, 1998). These further studies would enable us to evaluate the gas bubble behavior in magma quantitatively from observed geodetic data.

## 8. Conclusion

We examined basic characteristics of temporal changes of ground deformation generated by magma ascent in an open conduit that produces small repeated and intermittent explosions. Theoretical considerations clarify the following points. Magma ascent, derived as a Poiseuille flow without gas bubble growth, generates an almost constant increase or gradual decrease in amplitudes of ground deformation at far fields. In contrast, gas bubble behavior in the melt accelerates ground deformation. The amplitudes of displacements and tilt are proportional to the 1.5 power of time when gas bubbles in magma expand by diffusive mass transfer of water molecules in the melt. Rapidly increased volcano inflation is observed when gas bubbles rise in a low-viscosity melt because of buoyancy. These predictions of temporal changes in ground deformations aid the interpretation of the observed inflations accompanying intermittent eruptions and ease understanding of the mechanisms of magma ascent in open conduits. Furthermore, data from dense geodetic networks are used to evaluate some physical parameters that quantitatively control microscale phenomena such as diffusion parameters of magma.

## Acknowledgements

This paper was improved as a result of stimulative discussions by Maurizio Ripepe and Mie Ichihara. Careful comments from two anonymous reviewers significantly improved this manuscript, and critical comments from one reviewer improved the understanding of the magma pressure distribution in the conduit after the eruptions. This study was partly supported by the G-COE program of Tohoku University “Global Education and Research Center for Earth and Planetary Dynamics”.

## Appendix A. Initial magma pressure distribution in the conduit after eruptions

Spatio-temporal distribution of magma in the conduit just after eruptions shown in Fig. 2 is examined from numerical calculation results obtained from a simple magma flow model. Here, we assume com-

pressible magma in a cylindrical pipe without gas bubble behavior, although magma behavior in the conduit during the eruptions includes complex processes of gas bubble growth, coalescence and collapse. The basic equations of the flow are the conservation of mass and the conservation of momentum, which are written as:

$$\frac{\partial \rho}{\partial t} = -\frac{\partial}{\partial z}(\rho v), \quad (\text{A1})$$

$$\frac{\partial v}{\partial t} + v \frac{\partial v}{\partial z} = -\frac{1}{\rho} \frac{\partial p}{\partial z} + g - \frac{8\eta}{\rho a^2} v, \quad (\text{A2})$$

where  $z$  represents the depth of magma,  $t$  is the time,  $\rho$ ,  $v$  and  $p$  are the density, velocity, and pressure of magma, respectively,  $\eta$  is the magma viscosity,  $a$  is the conduit radius, and  $g$  is the gravitational acceleration. Downward direction is positive in the  $z$ -axis. Compressibility of magma is expressed as a relation between the pressure and density:

$$\rho = \rho_r \left(1 + \frac{p - p_r}{K}\right), \quad (\text{A3})$$

where  $\rho_r$  is the reference magma density at the pressure  $p_r$ , and  $K$  is the bulk modulus of magma. Normalizing the parameters in Eqs. (A1)–(A3) by using  $z' = z/L$ ,  $t' = t/(L/c_0)$ ,  $\rho' = \rho/\rho_r$ ,  $p' = p/(\rho_r g L)$  and  $K' = K/(\rho_r g L)$ , where  $c_0 \equiv \sqrt{K/\rho_r}$  and  $L$  is the conduit length, we obtain

$$\frac{\partial \rho'}{\partial t'} = -\frac{\partial}{\partial z'}(\rho' v'), \quad (\text{A4})$$

$$\frac{\partial v'}{\partial t'} + v' \frac{\partial v'}{\partial z'} = -\frac{1}{\rho'} \frac{\partial p'}{\partial z'} + \frac{1}{K'} - \frac{\beta v'}{K' \rho'}, \quad (\text{A5})$$

where

$$\beta = \frac{8\eta c_0}{\rho_r g a^2} \quad (\text{A6})$$

is the non-dimensional parameter determining viscous property of the magma flow system: large and small  $\beta$  represents high and low viscous flow, respectively.

Just before eruption, the magma pressure at the top is pressurized at  $p_{\text{atm}} + \delta p$ , and the magma pressure almost linearly increases with

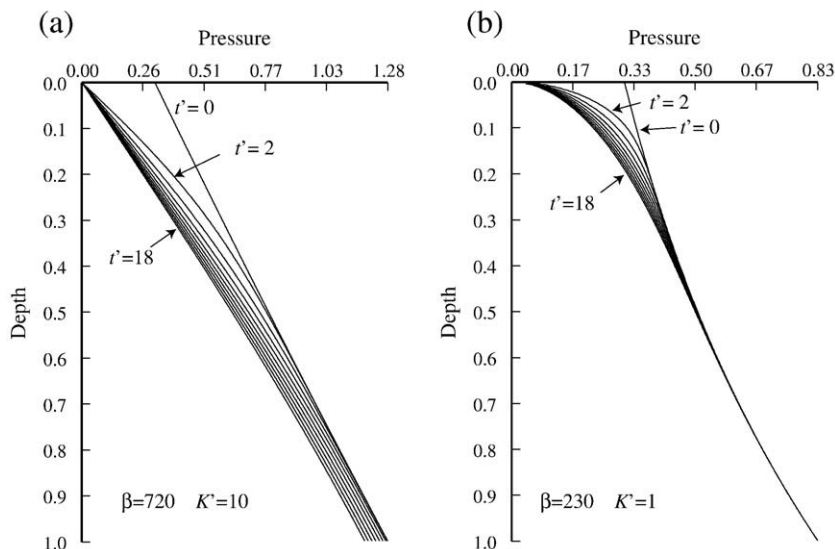


Fig. A1. Spatio-temporal changes of the magma pressure in the conduit after the eruption. (a)  $\beta = 720$  and  $K' = 10$  and (b)  $\beta = 230$  and  $K' = 1$ .

depth due to the overburden pressure of magma itself. An eruption is triggered by setting the magma pressure at the top of the conduit to be  $p_{\text{atm}}$  at  $t=0$ . At the bottom of conduit, magma velocity is always set to be zero, that is, no supply of magma from a deeper part.

Two parameters  $\beta$  and  $K'$  determine the behavior of magma motions in the conduit as indicated in Eqs. (A4)–(A5). Fig. A1 shows examples of spatio-temporal changes of the magma pressure in the conduit: (a)  $\beta=720$  and  $K'=10$  and (b)  $\beta=230$  and  $K'=1$ . The overpressure of  $\delta p'=0.3$  is assumed. Fig. A1a shows an example of rapid decrease of the magma pressure. The magma pressure at the bottom starts to decrease almost at  $t'=1$ , which is the time when the pressure waves propagating with the acoustic velocity of magma arrives at the bottom. In this case, the pressure wave propagation is the main factor decreasing the magma pressure in the conduit. On the other hand, Fig. A1b indicates that the magma pressure slowly decreases with time from the top to the bottom of the conduit. Even at time  $t'=18$ , lower half portions of the conduit keep the initial magma pressure, which is similar to the spatio-temporal distribution shown in Fig. 2d. These results suggest that the spatio-temporal changes of magma pressure in the conduit depends on the magma property and conduit radius.

To quantitatively understand the effect of magma property on the depressurization in the conduit, we measure the start time of depressurization at the bottom of conduit by substituting plausible physical properties of magma and conduit in Eqs. (A1)–(A3). The conduit radius of 2 m, the magma density of  $2000 \text{ kg/m}^3$ , the conduit length of 5000 m and  $g$  of  $9.8 \text{ m/s}^2$  are assumed. We vary the magma viscosity from  $10^3$  to  $10^5 \text{ Pa s}$ . The bulk modulus of liquid magma is about  $10^{10} \text{ Pa}$ , but tiny gas bubbles in magma can significantly decrease the bulk modulus of magma. For example, the bulk modulus of magma with a gas volume fraction of 0.05 is about  $10^8 \text{ Pa}$  at shallow parts (e.g., Aki et al., 1978). Supposing that these tiny gas bubbles do not affect the magma flow in the conduit, we change the bulk modulus of magma from  $10^8$  to  $10^{10} \text{ Pa}$ . As a result, the acoustic velocity of magma is ranging from about 200 to 2000 m/s. Fig. A2 plots a contour map of the start time of depressurization for the viscosity and bulk modulus of magma. The start time of depressurization is defined as the time when the magma pressure at the bottom decreases 0.1 % from the initial value. We set the overpressure  $\delta p$  to be 30 MPa (this value corresponds to  $\delta p'=0.3$ ). It is found that the start time of depressurization is quite small for the magma with a low viscosity and

large bulk modulus. The start time of depressurization is less than 1 min for, for example,  $\eta < 10^4 \text{ Pa s}$  and  $K > 10^9 \text{ Pa}$  (right and lower part of Fig. A2). In these ranges of magma property, the magma pressure in the conduit rapidly decreases just after eruption, which corresponds to Fig. 2b. On the other hand, when the magma is characterized by high viscosity and low bulk modulus, the start time of depressurization becomes longer. For example, for  $\eta > 10^4 \text{ Pa s}$  and  $K < 5 \times 10^8 \text{ Pa}$ , the start time of depressurization increases from a few minutes to several tens of minutes. The start time of depressurization decreases (or increases) for the conduit with a larger (or smaller) radius, as suggested from Eq. (A5).

## References

- Aki, K., Chouet, B., Fehler, M., Zandt, G., 1978. Seismic properties of a shallow magma reservoir in Kilauea Iki by active and passive experiments. *J. Geophys. Res.* 83, 2273–2282.
- Barmin, A., Melnik, O., Sparks, R.S.J., 2002. Periodic behavior in lava dome eruptions. *Earth Planet. Sci. Lett.* 199, 173–184.
- Beauducel, F., Cornet, F.-H., Suhanto, E., Duquesnoy, T., Kasser, M., 2000. Constraints on magma flux from displacements data at Merapi volcano, Java, Indonesia. *J. Geophys. Res.* 105, 8193–8203.
- Bonaccorso, A., Davis, P.M., 1999. Models of ground deformation from vertical volcanic conduits with application to eruptions of Mount St. Helens and Mount Etna. *J. Geophys. Res.* 104, 10,531–10,542.
- Cayol, V., Cornet, F., 1998. Effects of topography on the interpretation of the deformation field of prominent volcanoes – application to Etna. *Geophys. Res. Lett.* 25, 1979–1982.
- Chadwick Jr., W.W., Archuleta, R.J., Swanson, D.A., 1988. The mechanism of ground deformation precursory to dome-building extrusions at Mount St. Helens 1981–1982. *J. Geophys. Res.* 93, 4351–4366.
- Chouet, B., Dawson, P., Nakano, M., 2006. Dynamics of diffusive bubble growth and pressure recovery in a bubbly rhyolitic melt in an elastic solid. *J. Geophys. Res.* 111. doi:10.1029/2005JB004174.
- Dzurizun, D., Westphal, J.A., Johnson, D.J., 1983. Eruption prediction aided by electronic tiltmeter data at Mount St. Helens. *Science* 221, 1381–1383.
- Green, D.N., Neuberg, J., Cayol, V., 2006. Shear stress along the conduit wall as a plausible source of tilt at Soufrière Hills volcano, Montserrat. *Geophys. Res. Lett.* 33. doi:10.1029/2006GL025890.
- Harris, A.J.L., Rippepe, M., 2007. Temperature and dynamics of degassing at Stromboli. *J. Geophys. Res.* 112. doi:10.1029/2006JB004393.
- Ida, Y., 2007. Driving force of lateral permeable gas flow in magma and the criterion of explosive and effusive eruptions. *J. Volcanol. Geotherm. Res.* 162, 172–184.
- Iguchi, M., Yakiwara, H., Tameguri, T., Hendrasto, M., Hirabayashi, J., 2008. Mechanism of explosive eruption revealed by geophysical observations at the Sakurajima, Suwanosejima and Semeru volcanoes. *J. Volcanol. Geotherm. Res.* 178, 19.
- Ishihara, K., 1985. Dynamical analyses of volcanic explosion. *J. Geodynamics* 3, 327–349.
- Jackson, P., et al., 1998. Ground deformation studies at Soufrière Hills Volcano, Montserrat I: electronic distance meter studies. *Geophys. Res. Lett.* 25, 3409–3412.
- Jaupart, C., Allègre, C.J., 1991. Gas content, eruption rate and instabilities of eruption regime in silicic volcanoes. *Earth Planet. Sci. Lett.* 102, 413–429.
- Jaupart, C., Vergnolle, S., 1988. Laboratory models of Hawaiian and Strombolian eruptions. *Nature* 331, 58–60.
- Lautze, N.C., Houghton, B.F., 2007. Linking variable explosion style and magma textures during 2002 at Stromboli volcano, Italy. *Bull. Volcanol.* 69, 445–460.
- Lensky, N.G., Navon, O., Lyakhovsky, V., 2004. Bubble growth during decompression of magma: experimental and theoretical investigation. *J. Volcanol. Geotherm. Res.* 129, 7–22.
- Lyakhovsky, V., Hurwitz, S., Navon, O., 1996. Bubble growth in rhyolitic melts: experimental and numerical investigation. *Bull. Volcanol.* 58, 19–32.
- Manga, M., 1996. Waves of bubbles in basaltic magmas and lavas. *J. Geophys. Res.* 101, 17,457–17,465.
- Mason, R.M., Starostin, A.B., Melnik, O.E., Sparks, R.S.J., 2006. From Vulcanian explosions to sustained explosive eruptions: the role of diffusive mass transfer in conduit flow dynamics. *J. Volcanol. Geotherm. Res.* 153, 148–165.
- Melnik, O., Sparks, R.S.J., 1999. Nonlinear dynamics of lava dome extrusion. *Nature* 402, 37–41.
- Mogi, K., 1958. Relations between the eruptions of various volcanoes and the deformations of the ground surfaces around them. *Bull. Earthquake Res. Inst. Univ. Tokyo* 36, 99–134.
- Nakanishi, M., Koyaguchi, T., 2008. A stability analysis of a conduit flow model for lava dome eruptions. *J. Volcanol. Geotherm. Res.* 178, 46–57.
- Nishi, K., Hendrasto, M., Mulyana, I., Rosadi, U., Purbawinata, M.A., 2007. Micro-tilt changes preceding summit explosions at Semeru volcano, Indonesia. *Earth Planets Space* 59, 151–156.
- Nishimura, T., 2004. Pressure recovery in magma due to bubble growth. *Geophys. Res. Lett.* 31. doi:10.1029/2004GL019810.
- Nishimura, T., 2006. Ground deformation due to magma ascent with and without degassing. *Geophys. Res. Lett.* 33. doi:10.1029/2006GL028101.
- Nishimura, T., Chouet, B., 2003. A numerical simulation of magma motion, crustal deformation, and seismic radiation associated with volcanic eruptions. *Geophys. J. Int.* 153, 699–718.

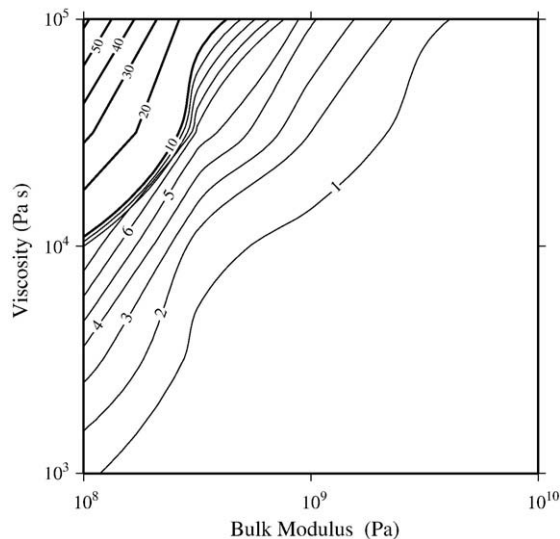


**Fig. A2.** Start times of depressurization of the conduit bottom for various magma viscosity and bulk modulus. Thin and thick lines represent contour lines with an interval of 1 min and 10 min., respectively. The contour lines of 1 min interval are abbreviated over 10 min.

- Nishimura, T., Ichihara, M., Ueki, S., 2006. Investigation of the Onikobe geyser, NE Japan, by observing the ground tilt and flow parameters. *Earth Planets Space* 58, e21–e24.
- Ohminato, T., Takeo, M., Kumagai, H., Yamashina, T., Oikawa, J., Koyama, E., Tsuji, H., Urabe, T., 2006. Vulcanian eruptions with dominant single force components observed during the Asama 2004 volcanic activity in Japan. *Earth Planets Space* 58, 583–593.
- Okada, Y., 1992. Internal deformation due to shear and tensile faults in a half-space. *Bull. Seismol. Soc. Am.* 82, 1018–1040.
- Okumura, S., Nakamura, M., Tsuchiyama, A., 2006. Shear-induced bubble coalescence in rhyolitic melts with low vesicularity. *Geophys. Res. Lett.* 33. doi:10.1029/2006GL027347.
- Prousevitch, A.A., Sahagian, D.L., 1996. Dynamics of coupled diffusive and decompressive bubble growth in magmatic system. *J. Geophys. Res.* 101, 17,447–17,455.
- Prousevitch, A.A., Sahagian, D.L., Anderson, A.T., 1993. Dynamics of diffusive bubble growth in magmas: isothermal case. *J. Geophys. Res.* 98, 22,283–22,307.
- Ripepe, M., Harris, A.J.L., 2008. Dynamics of the 5 April 2003 explosive paroxysm observed at Stromboli by a near-vent thermal, seismic and infrasonic array. *Geophys. Res. Lett.* 35. doi:10.1029/2007GL032533.
- Saito, E., et al., 1993. Geodetic monitoring using EDM before and during the 1991–1992 lava extrusion of Fugen-dake, Unzen Volcano, Kyushu, Japan. *Bull. Geol. Surv. Japan* 44, 639–647 (in Japanese with English abstract).
- Shimomura, Y., Nishimura, T., Sato, H., 2006. Bubble growth processes in magma surrounded by elastic medium. *J. Volcanol. Geotherm. Res.* 155, 307–322.
- Tait, S., Jaupart, C., Vergnolle, S., 1989. Pressure, gas content and eruption periodicity of a shallow, crystallising magma chamber. *Earth Planet. Sci. Lett.* 92, 107–123.
- Takeuchi, S., Nakashima, S., Tomiya, A., Shinohara, H., 2005. Experimental constraints on the low gas permeability of vesicular magma during decompression. *Geophys. Res. Lett.* 32. doi:10.1029/2005GL022491.
- Tameguri, T., Iguchi, M., Ishihara, K., 2002. Mechanism of explosive eruptions from moment tensor analyses of explosion earthquakes at Sakurajima Volcano, Japan. *Bull. Volcanol. Soc. Jpn.* 47, 197–215.
- Toramaru, A., 1989. Vesiculation process and bubble size distributions in ascending magmas with constant velocities. *J. Geophys. Res.* 94, 17523–17542.
- Voight, B., et al., 1999. Magma flow instability and cyclic activity at Soufriere Hills volcano, Montserrat, British West Indies. *Science* 283, 1138–1141.
- Voight, B., et al., 2000. Deformation and seismic precursors to dome-collapse and fountain-collapse nuées ardentes at Merapi Volcano, Java, Indonesia, 1994–1998. *J. Volcanol. Geotherm. Res.* 100, 261–287.
- Voight, B., et al., 2006. Unprecedented pressure increase in deep magma reservoir triggered by lava-dome collapse. *Geophys. Res. Lett.* 33. doi:10.1029/2005GL024870.
- Woods, A.W., Koyaguchi, T., 1994. Transitions between explosive and effusive eruptions of silicic magmas. *Nature* 370, 641–644.
- Wylie, J.J., Voight, B., Whitehead, J.A., 1999. Instability of magma flow from volatile-dependent viscosity. *Science* 285, 1883–1885.
- Yamashina, K., Shimizu, H., 1999. Crustal deformation in the mid-May 1991 crisis preceding the extrusion of a dacite lava dome at Unzen volcano, Japan. *J. Volcanol. Geotherm. Res.* 89, 43–55.
- Yoshida, S., Koyaguchi, T., 1999. A new regime of volcanic eruption due to the relative motion between liquid and gas. *J. Volcanol. Geotherm. Res.* 89, 303–315.

## 木管楽器（リコーダー）に学ぶ火山性微動発生機構の考察

○市原美恵（東大・地震研）・佐藤元彦・宮林佐和子（東大・理）  
武尾実・綿田辰吾（東大・地震研）・井口正人（京大・防災研）

## From a musical recorder to insights of volcanic tremor

Mie Ichihara (ERI, Univ. of Tokyo), Motohiko Sato, Sawako Miyabayashi (Grad. Sch. Sci., Univ. of Tokyo)

Minoru Takeo, Shingo Watada (ERI, Univ. of Tokyo), Masato Iguchi (DPRI, Kyoto Univ.)

## 1. はじめに

火山活動に伴って発生する特徴的な地震現象のひとつに、ハーモニック型微動があるが、その発生機構はまだ解明されていない。これまでに行われた研究は、スペクトルのピークの位置を説明する共鳴体の構造や物性を議論したもの (Chouet, 1986; Fujita & Ida, 2003; Kumagai & Chouet, 2000 等) と、流体の流れから持続的な周期振動を励起する非線形システムを議論したものの (Julian, 1994; Fujita et al., 2004) に大きく分けられる。本研究では、身近な楽器であるリコーダーのメカニズムに発想を得て、ハーモニック振動の発生過程における共鳴体と励起源のカップリングについて考察する。

## 2. リコーダー

リコーダーは、空気を空洞に吹き込んで音を発生させるフルート型の楽器のひとつであり、音の発生機構や、音高・音色を支配する要素は、理論的にもよく分かっている。簡単に言えば、口から吹き込む空気ジェットが、ジェットと周囲気体との速度勾配によって励起され、それが共鳴管内の圧力振動とカップルして安定的に振動が継続するというこららしい (Fletcher & Rossing, 1998)。発振周波数の理論計算では、管の構造でほぼ決まる共鳴周波数の位置と、ジェットのダイナミクスで決まる振動エネルギー供給条件が考慮される。

## 3. 実験方法と結果

リコーダーの指穴は全て塞ぎ、コンプレッサーから圧力調整弁を通して空気を吹き込む。もう一方の端は開放端にするか、水につけて長さを調節する。発生する音と、吹込圧力・管長の関係を調べる。吹込圧力をゆっくり増加させると、共鳴周波数は階段状に不連続に増加する (Fig.1)。一方、管をだんだん長くすると、共鳴周波数は連続的に低下したかと思うと、急に高い周波数が現れる (Fig.2)。これらの振る舞いは、先述の理論計算でも再現できる。さらに、不連続な変化のところで変化前後のモードが重なる場合のあること、ジェット速度が音速を超える、吹込圧力 60 kPa 付近で分岐のような現象が見える (Fig.1) 現象などは、実験で新たに分かったことである。

## 4. 火山性微動への応用

本研究の結果、ハーモニック振動の発振機構について、新たな知見が得られた。特に、連続的なパラメータの変化により、周波数が不連続に飛ぶこと、共鳴体の長さの増加により、周波数が高くなることもあり得ることは、重要である。実際の火山性微動のスペクトルを見直してみると、リコーダーと同様の、不連続な周波数の変化や、モードの重なり合いが見られることに気付いた (Fig.3)。これらの特徴から、火山性微動の励起メカニズムに関する重要な情報を読み取ることができると期待している。

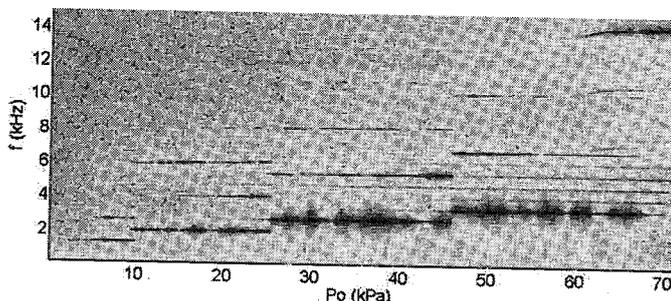


Fig.1 Recorder sound for changing blow pressure.

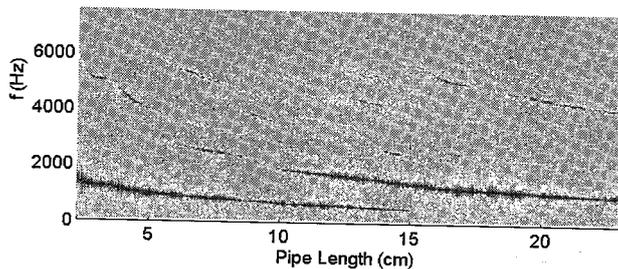


Fig.2 Recorder sound for changing length.

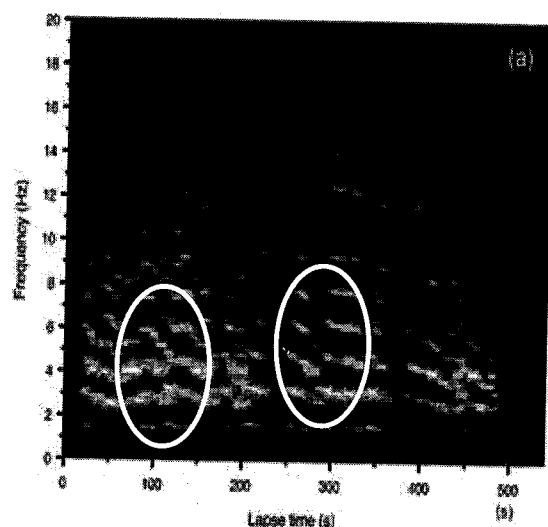


Fig.3 Volcanic tremor recorded at Sakurajima (HTB type). [Maryanto et al, 2008]